Adenylnucleotide-mediated binding of the PII-like protein SbtB contributes to controlling activity of the cyanobacterial bicarbonate transporter SbtA

Britta Förster [1]*, Bratati Mukherjee [1], Loraine M. Rourke [1], Joe A. Kaczmarski [2,3], Colin J. Jackson [b], G. Dean Price [1]

Author affiliations:
[1] ARC Centre of Excellence in Translational Photosynthesis, Division of Plant Sciences, Research School of Biology, The Australian National University, Canberra, Australia

[2] ARC Centre of Excellence in Synthetic Biology, Research School of Chemistry, The Australian National University, Canberra, Australia

[3] ARC Centre of Excellence for Innovations in Peptide and Protein Science, Research School of Chemistry, The Australian National University, Canberra, Australia

***For correspondence**: britta.forster@anu.edu.au

Key words: cyanobacteria, CO_2 concentrating mechanism, PII-like protein SbtB, bicarbonate transporter SbtA, protein-protein interaction, adenylate energy charge response

Abstract

Cyanobacteria have evolved a remarkably powerful CO_2 concentrating mechanism (CCM), enabling high photosynthetic rates in environments with limited inorganic carbon (Ci). Therefore, this CCM is a promising system for integration into higher plant chloroplasts to boost photosynthetic efficiency and yield. The CCM depends on active Ci uptake, facilitated by bicarbonate transporters and CO_2 pumps, to elevate CO_2 concentration around the active sites of the primary CO_2 fixing enzyme, Rubisco, which is encapsulated in cytoplasmic micro-compartments (carboxysomes). The essential CCM proteins have been identified, but the molecular signals and regulators that coordinate function in response to light, Ci availability and other environmental cues are largely unknown. Here, we provide evidence, based on a novel *in vitro* binding system, for a role of the PII-like SbtB protein in regulating Ci uptake by the bicarbonate transporter, SbtA, in response to the cellular adenylate energy charge (AEC) through dynamic protein-protein interaction. Binding of the SbtA and SbtB proteins from two phylogenetically distant species, *Cyanobium sp*. PCC7001 and *Synechococcus elongatus* PCC7942, was inhibited by high ATP, and promoted by low [ATP]:[ADP or AMP] ratios *in vitro*, consistent with a sensory response to the AEC mediated through adenylnucleotide ligand-specific conformation changes in SbtB. *In vivo*, cell cultures of S. elongatus showed up to 70% SbtB-dependent down-regulation of SbtA bicarbonate uptake activity specifically in the light activation phase during transitions from dark to low light when low cellular AEC is expected to limit metabolic activity. This suggests SbtB may function as a curfew protein during prolonged low cellular AEC and photosynthetically unfavourable conditions to prevent energetically futile and physiologically disadvantageous activation of SbtA.

Introduction

The cyanobacterial CO_2 concentrating mechanism (CCM) is one of the most efficient CCMs known to date. It has been fundamental to their adaptability and successful competition in environments providing limited inorganic carbon (Ci) supply for oxygenic photosynthesis and is reflected in an estimated contribution of 30-80% global primary productivity in the oceans (Liu et al., 1997; Field et al., 1998). Therefore, recent efforts to enhance photosynthetic carbon fixation in crop species have focussed on introducing a synthetic cyanobacterial CCM into chloroplasts, which has been predicted to translate into 36-60% higher crop productivity (Price et al., 2013; McGrath and Long, 2014; Long et al., 2016; Meyer et al., 2016). The cyanobacterial CCM enables active uptake of two Ci species, CO_2 and bicarbonate (HCO_3^-), which leads to accumulation of a cytoplasmic bicarbonate pool as large as 20-40 mM (Badger and Andrews, 1982; Price and Badger, 1989). This bicarbonate pool supports carbonic anhydrase (CA)-mediated elevation of the CO_2 concentration around the primary CO_2-fixing enzyme ribulose-1,5-bisphoshate carboxylase/oxygenase (Rubisco) inside proteinaceous micro-compartments

known as carboxysomes. Consequently, Rubisco carboxylation is enhanced over oxygenation, suppressing energetically costly photorespiration (for review see (Badger and Price, 1992; Kaplan and Reinhold, 1999; Price et al., 2008; Espie and Kimber, 2011; Price, 2011)). To date, five Ci uptake systems have been verified, varying with respect to energization, substrate affinity, flux rates and induction by low Ci conditions (Price, 2011). Two light-dependent, thylakoid-located CO_2 pumps or energy-coupled CAs, Ndh-1_3 and Ndh-1_4 (Maeda et al., 2002; Ohkawa et al., 2002), convert external and internally recaptured CO_2 to HCO_3^-, energized by NADPH and reduced ferredoxin (Ogawa et al., 1985; Maeda et al., 2002; Price et al., 2008). Three types of plasma membrane-located bicarbonate transporters, the ATP-dependent BCT1 complex (Omata et al., 1999) and the HCO_3^-/Na^+ symporters BicA (Price et al., 2004) and SbtA (Shibata et al., 2002), transfer bicarbonate directly from the external environment into the cytoplasm upon activation by low Ci conditions and light (Sültemeyer et al., 1998; McGinn et al., 2003). Of particular interest for a synthetic CCM is SbtA due to its ability to function in nonphotosynthetic *E. coli* (Du et al., 2014). SbtA requires a Na^+ gradient directed from the outside to the inside of the cell for activity (Shibata et al., 2002; Price et al., 2004). Both CO_2 uptake and HCO_3^- transport are activated by light within 5 and 30 s, respectively, (Badger and Andrews, 1982; Price et al., 2011). Early on, Kaplan *et al*. reported a gradual inactivation of Ci uptake in the dark, suggesting a link to the state of photosynthetic electron transport or a redox signal (Kaplan et al., 1987), but the molecular mechanisms regulating the activity of specific bicarbonate transporters are largely unknown.

A highly conserved feature of cyanobacterial genomes is the presence of the *sbtB* gene, encoding the PII-like SbtB protein, in the immediate gene neighbourhood of the *sbtA* gene (Rae et al., 2011). Both genes are co-expressed under Ci limitation in *Synechococcus elongatus* PCC7942 and *Synechocystis sp.* PCC 6803 (Woodger et al., 2003; Schwarz et al., 2011), suggesting a functional connection between the SbtA and SbtB proteins. This has been supported by evidence from co-expression of several SbtA and SbtB proteins in *E. coli*, where SbtA-mediated bicarbonate uptake was specifically inactivated in the presence of the cognate SbtB protein, and a physical interaction was shown for the SbtA and SbtB proteins from *S. elongatus* PCC7942 (hereafter $SbtA_{7942}$ and $SbtB_{7942}$, respectively) (Du et al., 2014). Similarly, a study by Selim *et al.* (Selim et al., 2018) indicated SbtA and SbtB from *Synechocystis sp.* PCC6803 (hereafter $SbtA_{6803}$ and $SbtB_{6803}$, respectively) interacted in response to Ci availability, which was enhanced by addition of ADP or AMP and diminished by cAMP. It was suggested the cAMP:AMP ratio may indirectly signal intracellular Ci levels and thus regulate $SbtA_{6803}$:$SbtB_{6803}$ complex formation, but effects on SbtA activity were not directly assessed. Meanwhile, a broader role for $SbtB_{6803}$ in Ci and metabolic sensing has emerged. The same study (Selim et al., 2018) showed that the *sbtB6803* knockout mutant was impaired in acclimation to high Ci conditions, remaining locked in the high Ci affinity state typical of low Ci acclimation. Moreover,

70 $SbtB_{6803}$ was implicated in far red light induced inhibition of photosynthetic oxygen evolution (Oren et
71 al., 2021) and in bis-(3′,5′)-cyclic diadenosine monophosphate (c-di-AMP) and redox state sensing
72 linked to control of glycogen synthesis and growth performance of cyanobacterial cells during
73 day/night cycles (Selim et al., 2021; Selim et al., 2023).
74 Structural evidence for SbtA:SbtB interaction comes from X-ray crystallography and cryo-electron
75 microscopy, which resolved trimeric $SbtA_{6803}$ bound to $SbtB_{6803}$ trimers in the presence of AMP as a
76 ligand to SbtB (Fang et al., 2021; Liu et al., 2021). Furthermore, SbtB proteins have been classified as
77 non-canonical PII-like members of the multi-functional PII and PII-like protein superfamily that consists
78 of transcriptional and protein activity regulators, environmental signal transducers or sensors, widely-
79 distributed across bacteria, archaea and plants (Radchenko et al., 2010). In cyanobacteria, there is
80 substantial evidence for a central role of PII proteins in sensing and balancing the carbon and nitrogen
81 status of the cell as part of regulatory networks that affect Ci and N acquisition (Forchhammer and
82 Selim, 2020). In crystals, SbtB proteins form homotrimers typical of PII with clefts between monomers
83 forming binding sites for small effector molecules (Forchhammer and Lüddecke, 2016) that may bind in
84 a competitive manner or cooperatively. Common ligands for PII proteins are ATP, ADP, Mg^{2+} and 2-
85 oxoglutarate (2OG) which impact on protein conformation, particularly the T-loop, and the interaction
86 with target proteins (Radchenko et al., 2010; Huergo et al., 2013; Zeth et al., 2014; Forchhammer and
87 Lüddecke, 2016; Forchhammer and Selim, 2020). Ligands for cyanobacterial PII-like proteins include
88 ADP and bicarbonate for the carboxysome-associated CPII from *Thiomonas intermedia* (Wheatley et
89 al., 2016), and adenylnucleotides for the $SbtB_{6803}$ protein, i.e. ATP, ADP, AMP, cAMP and c-di-
90 AMP(Selim et al., 2018; Selim et al., 2021) and the SbtB protein from *Cyanobium sp.* PCC7001
91 ($SbtB_{7001}$), i.e. cAMP, AMP, ADP, ATP and Ca^{2+}ATP (Kaczmarski et al., 2019). $SbtB_{6803}$ and $SbtB_{7001}$ share
92 the basic architecture, but differ in ligand-coordinating residues, ligand affinities and ligand-induced
93 conformation changes. Recently, $SbtB_{6803}$ was shown to exert apyrase activity, slowly converting ATP
94 ligands to AMP in a redox state-dependent manner (Selim et al., 2023). Apyrase activity was tightly
95 linked to the oxidation and disulfide bond formation between cysteines of the C-terminal R-loop,
96 which is an extension that is present on a subset of SbtB proteins but not in $SbtB_{7001}$ and $SbtB_{7942}$.
97 Therefore, one may expect fundamental mechanistic differences from $SbtB_{6803}$.
98 The energy status of living cells is reflected in the relative abundance rather than absolute
99 concentrations of the adenylnucleotides ATP, ADP and AMP and referred to as the cellular
100 adenylate energy charge (AEC), described quantitatively as ([ATP]+0.5[ADP])/([ATP]+[ADP]+[AMP])
101 (Chapman et al., 1971). Intriguingly, $SbtB_{7001}$ had 18 to 38-fold higher binding affinities for ATP over
102 ADP, AMP and cAMP in the presence of Ca^{2+} (Kaczmarski et al., 2019), which suggested to us certain
103 SbtB proteins may sense the AEC directly and dynamically interact with SbtA in response to changes in
104 adenylate nucleotide ratios. We propose that the adenylnucleotide ligand-induced structural changes

105 observed for SbtB proteins determine SbtA:SbtB complex formation and control of the SbtA activation
106 state. Here, we demonstrate that the adenylnucleotides ATP, ADP, AMP and cAMP regulate *in vitro*
107 binding of SbtA ($SbtA_{7001}$) from *Cyanobium sp.* PCC7001 and $SbtA_{7942}$ to their cognate SbtB proteins,
108 and present *in vivo* effects of SbtB on SbtA activity in cyanobacteria linked to light-induced changes in
109 AEC, consistent with a role of SbtB as AEC sensor and response regulator.
110

111 **Results**

112 **SbtA:SbtB complex formation is affected specifically by adenylnucleotides**

113 For SbtA:SbtB interaction studies, we co-expressed $SbtA_{7001}$, or $SbtA_{7942}$, with their cognate SbtB
114 proteins which were C-terminally tagged with human influenza hemagglutinin (HA) epitope and 5 or 6
115 histidines (His) in the *E.coli* strain DH5α (*E. coli*) and in a bicarbonate transporter-deficient
116 *Synechococcus elongatus* PCC7942 mutant (*Synechococcus* ΔCS). The $SbtB_{7001}$ and $SbtB_{7942}$ protein
117 were identified immunologically at 13 kDa, consistent with their calculated molecular weights, but the
118 apparent molecular weights of $SbtA_{7001}$ and $SbtA_{7942}$ monomers (23 kDa and 29 kDa, respectively) were
119 11 kDa lower than their calculated molecular weights, as is commonly observed for membrane
120 proteins and attributed to altered protein-SDS detergent interactions (Rath et al., 2009). Specific
121 binding of SbtA to SbtB proteins was evaluated *in vitro* by metal immobilized chromatography (IMAC)
122 using membrane-enriched, native protein extracts that contained both SbtA and HAHis-tagged SbtB
123 proteins (**Fig. S1**). Only the HAHis-SbtB but no SbtA protein was found to attach to Ni^{2+} coated beads
124 which ensured co-elution of SbtA and SbtB from the beads was exclusively due to the interaction of
125 the two proteins. The *in vitro* binding assays without addition of effectors showed that SbtA and SbtB
126 were largely dissociated in native protein extracts (**Figs. 1, S2**), which led us to focus on the association
127 of SbtA:SbtB complexes in response to a range of potential effector molecules and co-factors reported
128 to interact with PII and PII-like proteins. Based on our previous observation that $SbtB_{7001}$ binds ATP,
129 ADP, AMP and cAMP with micromolar affinities (Kaczmarski et al., 2019), we expected SbtA:SbtB
130 complex formation and dissociation be affected by these molecules. Since Ca^{2+} enhanced binding of
131 ATP to $SbtB_{7001}$ *in vitro* (Kaczmarski et al., 2019), we also included 200 nM Ca^{2+} in binding assays as a
132 potential cofactor, which was equivalent to the basal Ca^{2+} levels in cyanobacterial cells (Leganés et al.,
133 2009) did not facilitate SbtA:SbtB binding by itself (**Fig. S2**).
134 Under these conditions, the association of stable $SbtA_{7001}$:$SbtB_{7001}$ and $SbtA_{7942}$:$SbtB_{7942}$ complexes
135 was observed exclusively in the presence of 2 mM ADP or AMP (**Fig. 1**). Conversely, SbtA and SbtB
136 remained fully dissociated in the presence of 2 mM ATP or cAMP (**Fig. 1**).
137 In addition, a potential link between stabilization of SbtA:SbtB complexes and photosynthetic
138 activity was tested, but SbtA:SbtB binding was not affected by the Calvin-Benson-Basham (CBB) cycle

139 intermediates ribulose-1,5-bisphosphate (RUBP), 3-phosphoglycerate (3PGA) (**Fig. 2**). Similarly, 2OG
140 which is generated in the tricarboxylic acid (TCA) cycle and acts a master regulatory metabolite
141 coordinating carbon and nitrogen metabolism in association with canonical PII proteins (Huergo and
142 Dixon, 2015), did not facilitate SbtA:SbtB complex formation (**Fig. 2**).Combined with ATP or ADP, 2OG
143 had no synergistic effect (**Fig. 2**), in contrast to the prerequisite binding of Mg^{2+}ATP to the *E. coli* PII
144 protein for 2OG to become effective (Radchenko et al., 2013). Furthermore, we investigated possible
145 substrate-level regulation of SbtA activity via HCO_3^--dependent complex formation with SbtB. HCO_3^-
146 had no effect on SbtA:SbtB binding irrespective of combinations with Ca^{2+} or Mg^{2+}, ATP or AMP (**Fig.**
147 **S2, S3**). In summary, we observed that small molecule effectors unable to bind to $SbtB_{7001}$ (Kaczmarski
148 et al., 2019), were equally ineffective in mediating the binding of either SbtA-SbtB pair. It is notable
149 that SbtA-SbtB-effector interactions were very similar for proteins expressed in *E. coli* compared to
150 *Synechococcus* ΔCS (**Fig. 1, 2**), which suggests proteins were not subject to species-dependent, post-
151 translational modifications and validates use of *E. coli* as heterologous expression system.

152 **The AEC simulated by adenylnucleotide ratios determined the SbtA:SbtB complex formation**

153 The fact that SbtA:SbtB complexes were destabilized by ATP and stabilized by either ADP or AMP,
154 strongly suggested complex formation would be impacted by changes in the cellular adenylate energy
155 charge (AEC). Therefore, we simulated defined energy charge environments *in vitro* with different
156 molar ratios of ATP:ADP or ATP:AMP within a constant total adenylnucleotide pool of 2 mM. Both
157 SbtA-SbtB pairs, irrespective of expression in *E. coli* or *Synechococcus* ΔCS, showed decreasing
158 amounts of SbtA bound to SbtB with an increasingly higher proportion of ATP over ADP (**Fig. 3A-D**) and
159 AMP (**Fig. 3E,F**). Since both SbtA-SbtB pairs were unbound in the presence of cAMP (**Fig. 1**), we
160 replaced ATP with cAMP to test whether SbtA:SbtB binding could be affected by the molar ratios of
161 cAMP to ADP or AMP, similar to what has been reported for the $SbtA_{6803}$-$SbtB_{6803}$ pair (Selim et al.,
162 2018). It was indeed possible to impair SbtA:SbtB binding with high cAMP:ADP or AMP ratios (**Fig. 4**).
163 However, to evaluate the effects of cAMP in relation to ATP, it is important to recognize that ATP
164 concentrations up to 2 mM corresponded to the physiological range of intracellular ATP pools
165 measured in several bacteria (Thauer et al., 1977; Yaginuma et al., 2014), whereas estimates of cAMP
166 levels in cyanobacterial cells have been up to 1000-fold lower than the intracellular ATP levels, i.e. in
167 the nano- to micromolar range (Ohmori and Okamoto, 2004). The *in vitro* cAMP levels reducing the
168 amount of bound SbtA to 50% was 1.16 mM (**Fig. 5B**, AR_{50} of SbtA7942 cAMP:AMP) which is likely to
169 exceed the physiological range of intracellular concentrations by an order of magnitude. The lowest
170 tested cAMP to ADP or AMP ratio of 0.2 (95 µM cAMP : 1.905 mM ADP or AMP) is within
171 physiologically relevant range and cAMP did not affect the association of either SbtA-SbtB pair.
172 Therefore, changes in cAMP concentrations expected to occur *in vivo* are likely inconsequential
173 compared to the variations in intracellular ATP levels and the AEC.

174 To compare the association of SbtA with SbtB between adenylnucleotide treatments
175 quantitatively, we estimated the relative changes in SbtA abundance from densitometric analyses of
176 Western blot images (pixel volumes) against ATP:ADP or AMP and cAMP:ADP or AMP ratios (**Fig. S4**).
177 The association of SbtA with SbtB was non-linearly correlated with the adenylnucleotide ratio and
178 fitted best by a sigmoidal logistic model, typical of cooperative ligand binding (mean adjusted R^2 values
179 of 0.93 ± 0.02; **Fig. S4**). Comparing the adenylnucleotide ratios supporting 50% (AR_{50}) or 10% (AR_{10}) of
180 the maximum levels of SbtA bound to SbtB, derived from curve fits in **Fig. S4**, differences between the
181 two SbtA-SbtB pairs and in response to the four different adenylnucleotide combinations tested were
182 statistically not significant (**Fig. 5**). However, even though this implied very similar binding affinities of
183 $SbtB_{7001}$ and $SbtB_{7942}$ for those adenylnucleotides as well as comparable ligand-induced binding to the
184 cognitive SbtA proteins, $SbtA_{7942}$ seemed to be dissociated at slightly lower ATP:ADP, cAMP:ADP and
185 cAMP: AMP ratios than $SbtA_{7001}$.
186
187 **SbtA activity *in vivo* is modulated by SbtB and the light-stimulated adenylate energy charge**
188 Inside photosynthetic cyanobacterial cells, SbtA and SbtB proteins are both present when Ci
189 supply is low (**Fig. S1A**). In nonphotosynthetic *E. coli*, SbtA appeared to be constitutively inactivated in
190 the presence of SbtB (Du et al., 2014), which implied AEC levels were low under those experimental
191 conditions. In cyanobacteria, however, SbtA is active irrespective of SbtB when photosynthesis is fully
192 light-activated and cells operate at high AEC levels (**Figs. 6, S6, S7**). Therefore, it was of interest to
193 investigate SbtA function in low Ci combined with low AEC states which are prominent during dark-to-
194 low light transitions. Photosynthetic performance and uptake of ^{14}C-labelled HCO_3^- in *Synechococcus*
195 ΔCS expressing $SbtA_{7942}$ as the only HCO_3^- uptake system was compared either with or without $SbtB_{7942}$
196 (SbtAB and SbtA, respectively). Note that concurrent CO_2 uptake by Ndh-$1_{3/4}$ complexes was
197 eliminated by addition of the carbonic anhydrase inhibitor ethoxyzolamide (EZ), which does not affect
198 SbtA function (**Fig. S5**), and measurements were performed at pH 8.0 where HCO_3^- represents 98% of
199 the Ci pool. Under these conditions, the cells fully depended on SbtA activity for inorganic carbon
200 supply. At light intensities above the light compensation point, O_2 evolution rates directly reflected the
201 activity of $SbtA_{7942}$. In Ci-starved cell cultures steady-state photosynthetic rates in response to
202 incremental additions of bicarbonate were essentially the same for SbtA and SbtAB with substrate
203 affinities ($K_{0.5Ci}$; 9 ± 4 and 30 ± 5 µM Ci, respectively) and maximum rates of photosynthetic O_2
204 evolution (V_{maxO_2}; 164 ± 19 and 167 ± 12 µmol mg Chl*a* $^{-1}$ h $^{-1}$, respectively) (**Fig. S6**). Similarly,
205 alternating light intensities between 1400 and 200 µmol photons m^{-2} s^{-1} in the presence of saturating
206 Ci levels (250-500 µM) did not lead to discernible differences between SbtA and SbtAB in steady state
207 HCO_3^- uptake or photosynthetic O_2 evolution rates (**Fig. S7**). Together, this suggested SbtB is not

208 required for and does not regulate $SbtA_{7942}$ activity once photosynthesis has been fully activated in
209 response to light-intensity driven changes in carboxylation rates and Ci demand.
210 In contrast, SbtB clearly modulated SbtA function in the initial phase of dark-to-low light
211 transitions. After an hour of dark-adaptation, cells co-expressing SbtA and SbtB were unable to
212 activate $SbtA_{7942}$-dependent photosynthetic O_2 evolution to the same extent as cells expressing SbtA
213 alone during the initially low light phase of light response measurements, when light levels were below
214 or near the light compensation point of 10-15 µmol photons m^{-2} s^{-1} (**Fig. 6A**). Low light activation of ^{14}C-
215 labelled HCO_3^- uptake by $SbtA_{7942}$ clearly showed SbtA activation was strongly suppressed in the
216 presence of $SbtB_{7942}$ during the first 30-60 s after long-term dark-adaptation, reducing net SbtA activity
217 to 31% and 38% of the activity observed in the absence of SbtB at pH 8 and pH 9, respectively (**Fig. 6B**).
218 Since many photosynthetic processes are almost instantaneously inactivated in the dark, we tested
219 whether SbtB affected $[^{14}C]HCO_3^-$ uptake by $SbtA_{7942}$ during light to dark transition. Interestingly,
220 $SbtA_{7942}$ was fully inactivated within 15 s after cells were shifted from light into the dark without any
221 effect on the inactivation kinetics by the presence of the $SbtB_{7942}$ protein (**Fig. 6C**). Altogether this
222 suggests, SbtA activity is regulated at multiple levels, which may be SbtB-independent, but also involve
223 SbtB and AEC coupled regulation of SbtA activity demonstrated by dark-to-light activation kinetics of
224 SbtA.
225 In *Synechocystis sp.* PCC6803, deletion of $SbtB_{6803}$ was shown to reduce growth under low Ci
226 condition in low light (Selim et al., 2018), and a broader regulatory function of CCM components by
227 SbtB was proposed. If this was the case in *Synechococcus* ΔCS, one would expect a negative effect on
228 growth in cells expressing SbtA alone compared to those co-expressing SbtB and SbtA. However,
229 photoautotrophic growth of cells expressing either $SbtA_{7942}$ or both $SbtA_{7942}$and $SbtB_{7942}$, was very
230 similar when supplied with air levels of CO_2 under diurnal light-dark cycles (**Fig. S8**), suggesting deletion
231 of $SbtB_{7942}$, unlike $SbtB_{6803}$, did not impair photoautotrophic growth of *Synechococcus* ΔCS under the
232 conditions that provide a relatively stable light environment and sufficient CO_2 and nutrient supply.
233

234 **Discussion**

235 Allosteric regulation of cyanobacterial bicarbonate transporters has been an unresolved question for
236 quite some time with patchy evidence for diverse mechanisms and co-factors that may be involved. It
237 has already been established that SbtB is capable of exerting negative regulation on SbtA bicarbonate
238 uptake activity in a heterologous expression system (Du et al., 2014). Here, we provide evidence for
239 regulation of two SbtA bicarbonate transporters by protein-protein interaction with their cognate PII-
240 like SbtB proteins in response to the *in vitro* simulation and *in vivo* modulation of the adenylate energy
241 charge. The SbtA-SbtB pairs originated from the transitional α-cyanobacterium *Cyanobium sp.*
242 PCC7001 and the ß- cyanobacterium *Synechococcus elongatus* PCC7942, which are phylogenetically

243 relatively distant species (Rae et al., 2011; Sánchez-Baracaldo et al., 2019) but share overall sequence
244 homology at the amino acid level, with 60% identity between the two SbtA (**Fig. S9A, S10**) and 58%
245 identity between the two SbtB (**Fig. S9B, S11**) proteins. Importantly, the modelled structures of
246 $SbtA_{7001}$ compared to $SbtA_{7942}$ and $SbtB_{7001}$ compared to $SbtB_{7942}$ are nearly identical based on three-
247 dimensional models (**Fig. 7**). Together with convincingly similar interaction profiles for both SbtA-SbtB
248 pairs, we concluded they likely share the same overall regulatory mechanisms. It should be noted that
249 about 50% of the cyanobacterial SbtB family, which includes the SbtB proteins studied here, lack a
250 putative redox regulatory domain on the C-terminus, as typically found on SbtB of *Synechocystis sp.*
251 PCC6803 (Selim et al., 2023). This makes the present two SbtAB pairs a simpler system for studying the
252 nature of the primary signal(s) that direct allosteric inactivation/activation of SbtA.

253 **The AEC rather than cAMP is the probable primary effector determining SbtA:SbtB interactions**

254 Intracellular adenylnucleotide pools invariably contain ATP, ADP, AMP and cAMP, albeit relative
255 concentrations may vary rapidly dependent on metabolic activity in response to environmental and
256 developmental factors (De la Fuente et al., 2014). In cyanobacteria, cAMP is predominantly a
257 secondary messenger participating in different signalling events, whereas the relative abundances of
258 ATP, ADP and AMP define and communicate the cellular energy status. Notwithstanding, both
259 processes could translate Ci availability and Ci demand into SbtB-mediated regulation of SbtA. In
260 addition, relative abundances of cAMP, ATP and AMP in the adenylate pool are interdependently
261 influenced by the activities of adenylate cyclase and phosphodiesterases which catalyze cAMP
262 synthesis from ATP and hydrolytic degradation to AMP, respectively; depending on the species,
263 adenylate cyclase activity is stimulated by N and P deficiency, osmotic stress, light quality and in some
264 cases also bicarbonate or CO_2 (Cann, 2004; Hammer et al., 2006; Xu and Su, 2009; Agostoni and
265 Montgomery, 2014), potentially linking cAMP and Ci sensing.

266 Initially, evidence from *Synechocystis sp.* PCC6803 suggested the cAMP:AMP ratios determined
267 formation of SbtA:SbtB complexes and SbtA activity (Selim et al., 2018). $SbtB_{6803}$ was proposed to be a
268 novel cAMP receptor sensing the Ci status and mediating acclimation of the CCM to high Ci levels,
269 based on impaired acclimation in mutant cell lines lacking SbtB. In that study, high Ci acclimated cells
270 showed the expected general downregulation of Ci uptake alongside relatively higher cAMP levels and
271 cAMP:AMP ratios than in low Ci acclimated cells. However, $SbtB_{6803}$ was dissociated from $SbtA_{6803}$
272 which implied SbtA was inactive in its unbound state. Conversely, bicarbonate uptake was upregulated
273 in low Ci acclimated cells with high AMP levels and low cAMP:AMP ratios, which favoured formation of
274 SbtA:SbtB complexes, and therefore suggested SbtA was active when bound to SbtB. Those findings
275 were difficult to reconcile with the simple interaction model for SbtB-mediated SbtA regulation in *E.*
276 *coli*, where SbtA alone showed activity and co-expression of SbtA and SbtB inhibited SbtA-dependent

277 bicarbonate uptake, including the $SbtA_{6803}$-$SbtB_{6803}$ pair (Du et al., 2014). Meanwhile, regulation of
278 $SbtA_{6803}$ has been revised based on the finding that $SbtB_{6803}$ displays high affinity binding to SbtA only
279 with AMP as ligand and when the R-loop Cys residues are oxidized, which appeared to be the only
280 condition for T-loop conformation that permits binding to SbtA (Selim et al., 2023).
281 The binding analyses performed here (**Fig. 3**), and the fact that the R-loop is absent from $SbtB_{7001}$
282 and $SbtB_{7942}$ (**Fig. S9B**), clearly support the view that low levels of ATP and low ATP:ADP and AMP
283 ratios, representing a low AEC, determine the association of $SbtA_{7001}$- $SbtB_{7001}$ and $SbtA_{7942}$- $SbtB_{7942}$
284 pairs rather than cAMP levels and redox state of SbtB. Considering, that the cAMP concentrations that
285 effectively prevented the *in vitro* association of SbtA and SbtB were up to 1000-fold higher than
286 physiological levels of CAMP in cyanobacteria (Ohmori and Okamoto, 2004), it seems unlikely the
287 intracellular concentration of cAMP required for effective competition with ATP for binding sites on
288 SbtB would occur *in vivo*. Furthermore, the 6-12 times higher binding affinity of $SbtB_{7001}$ for ATP over
289 cAMP, ADP or AMP (Kaczmarski et al., 2019) is consistent with the proposed AEC-dependent regulation
290 of these SbtA-SbtB pairs. This AEC control of SbtA via binding/unbinding of SbtB might be a feature
291 across many cyanobacteria, but further experimentation is required to confirm this.
292
293 **The SbtA and SbtB proteins interact dynamically in response to the adenylate energy charge**
294 ATP, ADP and AMP form the core of the energy system of living cells. The majority of
295 biochemically available energy is linearly correlated with the molar fraction of ATP and ½ molar
296 fraction of ADP of the total adenylate pool, but was experimentally simplified here by testing effects of
297 ATP:ADP and ATP:AMP ratio effects separately (**Fig. 3**). Adenylate pools measured from a diverse range
298 of tissues, organisms and environmental conditions suggest active growth requires an adenylate
299 energy charge between 0.8 and 0.9, while a drop of the AEC below 0.5 is unsustainable (Chapman et
300 al., 1971). Under favourable environmental conditions, the AEC is kept remarkably steady near 0.8 in
301 cyanobacteria the light (Rust et al., 2011). Regulatory proteins often sense the AEC through
302 competitive binding of ATP or ADP (Atkinson and Walton, 1967), which includes PII proteins that
303 regulate target enzyme activity by undergoing specific conformational changes in response to binding
304 ATP or ADP, which alters the interaction between the PII protein and its target and modulates the
305 activity of the target protein (Radchenko et al., 2013; Zeth et al., 2014; Selim et al., 2019). This
306 principle also appears to apply to the interaction of the PII-like SbtB proteins with respective SbtA
307 transporters from both cyanobacterial species investigated. More than 90% of SbtA was unbound
308 (proposed active state) at a simulated AEC of 0.74 to 0.91 (**Figs. 3, 5**) approximating measured
309 ATP/(ATP+ADP) ratios of 0.8 to 0.9 reported for *Synechococcus elongatus* (formerly *Anacystis nidulans*)
310 ((Rust et al., 2011), recalculated from (Bornefeld and Simonis, 1974)) and the thermophile
311 *Synechococcus* strain Y-7c-s in medium light (250-270 µmol m^{-2} s^{-1}) (Kallas and Castenholz, 1982). This

312 suggests, in the light, photosynthetically active cyanobacterial cells would maintain an almost fully
313 active pool of SbtA, if the AEC was the defining parameter. The fact that $SbtA_{7942}$ activity was the same
314 for photosynthetically fully activated *Synechococcus* ΔCS strains expressing either SbtA or SbtA and
315 SbtB (**Fig. S6**, **S7**) supports the notion that SbtB had in fact fully dissociated from SbtA and did not limit
316 SbtA activity at high AEC. Without photosynthetic ATP production in the dark, or during excessive
317 cellular energy demand such as sudden decreases in light intensity and nutrient, pH or temperature
318 stress, the AEC is likely to decrease substantially in cyanobacterial cells. In *S. elongatus*, the ATP:ADP
319 ratio, was reduced to 0.55-0.6 about 10 min after light to dark transfer (Kallas and Castenholz, 1982;
320 Rust et al., 2011). Based on our *in vitro* binding analysis, this suggests, on average more than 50% of
321 both SbtA7001 and SbtA7942 should be bound to their respective SbtB proteins and form a stably-
322 inactivated SbtA pool in prolonged darkness. During light exposure, after long dark periods, it can take
323 from seconds to minutes for the cellular AEC to reach 0.8-0.9, dependent on light intensity and
324 activation of CO_2 fixation by Rubisco and the CBB cycle enzymes. Indeed, low light (70-100 µmol m^{-2} s^{-1})
325 did not increase the AEC beyond 0.6 in thermophilic *Synechococcus* (Kallas and Castenholz, 1982).
326 Importantly, when *Synechococcus* ΔCS strains expressing either SbtA or SbtA and SbtB were analysed
327 in dark-to-low light transitions, equivalent to raising AEC ratios from about 0.5 to 0.8-0.9, we detected
328 a transient and marked retardation in SbtA-dependent bicarbonate uptake, decreasing SbtA activity by
329 60-70% when SbtB was present compared to SbtA alone in the initial low light (30-50 µmol m^{-2} s^{-1})
330 phase (**Fig. 6A, B**). Assuming an AEC of 0.6 in low light, similar to Kallas *et al*., around 50% of SbtA
331 should still have been associated with SbtB (**Figs. 3, 5**). In our view, this is a convincing indication that a
332 rise in AEC is needed to displace the inhibitory SbtB curfew protein for SbtA activation during this
333 transition and that this takes a few seconds to achieve. Despite the technical difficulty, future work
334 looking at correlations between time-resolved AEC changes and bicarbonate uptake in *Synechococcus*
335 ΔCS strains should be able to test this further.
336

337 **Adenylnucleotide-dependent conformation changes of SbtB aligns with regulatory binding to SbtA**

338 Structural information of SbtA:SbtB complexes and binding of adenylate ligands to SbtB strongly
339 support the aforementioned AEC-dependent regulation of the SbtA:SbtB interaction *in vitro*.
340 Inevitably, uncertainty exists in extrapolating from *in vitro* findings to implications for *in vivo*
341 regulation. However, the case of regulation of SbtA by adenylate charge is at least feasible, especially
342 for the significant class of SbtA-SbtB-containing species that lack the putative C-terminal redox
343 regulatory domain on SbtB. The core structures and key amino acids involved in ligand binding that are
344 thought to facilitate SbtA:SbtB interactions are highly conserved between crystal structures of $SbtB_{6803}$
345 and $SbtB_{7001}$ and homology models of $SbtB_{7942}$ (**Figs. 7B,C, S10**) as well as crystallized $SbtA_{6803}$ and
346 homology models of $SbtA_{7001}$ and $SbtA_{7942}$ (**Figs. 7A,C, S10A, S12**), which lends some validity to propose

347 a generalized model for the regulatory interaction of subsets of those SbtB proteins missing the R-loop
348 and their cognate SbtA proteins. In PII proteins, the surface-exposed, flexible T-loop has been shown to
349 mediate the regulatory interaction with target protein(s). Upon binding small effector molecules,
350 ligand-induced conformation changes determine whether PII binds to its target. For example, binding
351 of ATP to the PII protein from *Synechococcus elongatus* PCC7942 induced T-loop conformation changes
352 that facilitated association with N-acetyl-glutamate kinase (NAGK) and arginine synthesis (Zeth et al.,
353 2014; Selim et al., 2019), and the ADP-stabilized T-loop of the PII protein GlnK from *E. coli* enable
354 formation of an inactivating complex with the ammonium transporter AMTB (Radchenko et al., 2010).
355 Crystallographic data support a direct correlation, analogous to PII proteins, between adenylate-ligand
356 induced changes in T-loop conformation of SbtB proteins (Selim et al., 2018; Kaczmarski et al., 2019;
357 Fang et al., 2021; Selim et al., 2023) and can explain the opposite effects of ATP and ADP or AMP on
358 SbtA:SbtB binding described here. The probability for each adenylate ligand to occupy a nucleotide
359 binding site would depend on the binding affinity and the local concentration of the ligand. At high
360 ATP:ADP or AMP ratios, when predominantly Ca^{2+}ATP is likely to occupy the nucleotide binding sites of
361 the $SbtB_{7001}$ trimers, the T-loops are probably stabilized (**Fig. 7B,C**) through interactions of specific
362 residues with the γ-phosphate of ATP, in a position close to the core overlapping the binding site
363 (Kaczmarski et al., 2019). When superimposed onto $SbtB_{6803}$ in the trimeric SbtA-SbtB cryo-EM
364 structure, it becomes apparent that the Ca^{2+}ATP-induced stable T-loop conformation of $SbtB_{7001}$
365 interferes with binding to SbtA (**Fig. 7D**), which would allow SbtA to be fully active. In contrast, at low
366 ATP:ADP or AMP ratios, occupation of the binding site mostly by ADP or AMP (**Fig. 7B,C**) would leave
367 the T-loops in a disordered or extended conformation (Kaczmarski et al., 2019; Fang et al., 2021),
368 which would enable formation of inactivated SbtA:SbtB complexes.

369

370 **A proposed model implicating SbtB in the regulation of SbtA activity in cyanobacteria**

371 For cyanobacteria, it is a selective advantage to maximize photosynthetic CO_2 fixation and carbon gain
372 for growth in the light. In the dark, photosynthetic CO_2 fixation ceases making Ci acquisition redundant
373 and energetically futile. Additionally, continued accumulation of large amounts of bicarbonate may
374 disrupt intracellular pH and ion homeostasis, particularly if $[Na^+]$ were to build up by HCO_3^-/Na^+
375 symport due to SbtA activity. Therefore, the co-ordinated regulation of Ci acquisition and
376 photosynthetic activity may be an imperative for optimal survival and success of cyanobacteria. A
377 hypothetical scenario for the regulation of bicarbonate uptake by SbtA in cyanobacteria is depicted in
378 **Fig. 8**, assuming functional units of both SbtA and SbtB proteins are trimers as indicated by cryo-EM
379 and crystal structures (Kaczmarski et al., 2019; Fang et al., 2021). In *Synechococcus*, SbtA function is
380 subject to several regulatory mechanisms operating at different time scales. In constant light and

381 stress-free environments, bicarbonate uptake rates of SbtA are clearly a product of light intensity and
382 Ci availability, independent of the SbtB protein (**Figs. 6**, **S7**). In light/dark cycles, SbtA is turned on and
383 off within a few seconds (**Fig. 6C**) in sync with the light-induced changes in Ci demand for
384 photosynthetic carboxylation, likely preventing the aforementioned complications associated with
385 bicarbonate and Na^+ over-accumulation. The nature of the signals and signal transduction pathways
386 triggering the fast activation-deactivation kinetics of SbtA may be complex and cannot be precisely
387 known at this stage, but some details can be envisaged. SbtA-mediated bicarbonate uptake is
388 immediately inactivated after a light-dark transition supposedly associated with a drop in the AEC,
389 assuming a similar decrease of the ATP/(ATP+ADP) ratio from 0.85 to about 0.4 observed in *S.*
390 *elongatus* previously (Bornefeld and Simonis, 1974; Takano et al., 2015). If AEC-induced binding of
391 SbtB was the primary inactivation mechanism during the light-to-dark transition, one would expect de-
392 regulation of SbtA activity in the absence of SbtB. Yet, SbtA-mediated bicarbonate uptake ceased
393 within 15 s in the dark irrespective of the presence of SbtB (**Fig. 6C**), which suggested the initial fast
394 inactivation of SbtA may be mediated by any one or a combination of other signals derived from the
395 many dark-induced changes in the cell which may involve the more oxidized redox state (Tamoi et al.,
396 2005), changes in net availability of ATP, in plasma membrane energization potentially involving Ca^{2+}
397 signalling (Torrecilla et al., 2004), in the transmembrane Na^+ gradient, and in protein post-translational
398 modifications such as phosphorylation (Spät et al., 2015; Angeleri et al., 2016). Many of these changes
399 are likely faster than a possible low-AEC-induced SbtA:SbtB association. On the other hand, we did
400 detect significant differences in the activation of bicarbonate uptake upon transition from dark to light
401 (Fig. 6), indicating low AEC-induced formation of inactive SbtA:SbtB complexes in the dark delayed
402 activation of SbtA until light-dependent increase in AEC was sufficient to facilitate the dissociation of
403 SbtB and SbtA.
404
405 **Conclusion**
406 The adenylate-specific binding of SbtB to SbtA suggests that *in vivo* SbtA trimers become locked
407 into an inactive state when the cellular adenylate energy charge is low, as is the case in low light or
408 darkness. This becomes evident from delay of SbtB-dependent re-activation of SbtA. According to our
409 hypothesis, low AEC-induced binding of SbtB to SbtA provides a curfew mechanism that ensures SbtA
410 activity is tuned to the capacity for photosynthetic C-fixation and tied to the energy resources
411 available. This mechanism may have evolved to override environmental and intrinsic cues that may
412 otherwise induce futile activation/inactivation cycles or activation of SbtA under conditions that
413 demand strategic investment of energy in cell survival rather than maximum growth. Limited light,
414 prolonged nutrient stress or environmental stress may require channelling of resources into
415 maintenance and protective processes instead of maximum photosynthesis and Ci accumulation. It will

416 be of interest to investigate to which extent AEC/SbtB-mediated regulation SbtA has been adopted
417 across cyanobacterial species. The general mechanism of energy charge-sensing via SbtB and its
418 interaction with SbtA is increasingly supported by experimental evidence, however, the precise details
419 are far from being fully understood. Further elucidation of molecular and biochemical mechanisms and
420 further substantiation of the role of the AEC in SbtA:SbtB complex formation *in vivo* under different
421 environmental conditions are challenges for future work. Nonetheless, the link between SbtB as a
422 sensor of the cellular energy status and response regulator of SbtA activity is an important novel
423 insight which may aid development of informed strategies for expression of SbtA-SbtB systems in
424 higher plant chloroplasts.
425

426 **Materials and Methods**

427 **Bacterial and cyanobacterial cell lines**

428 Nucleotide and amino acid sequences were retrieved from the Integrated Microbial Genome
429 database (IMG; https://img.jgi.doe.gov) and are referred to by gene ID and Locus_tags. The
430 commercially available *Escherichia coli* strain DH5α (Invitrogen) was used for cloning and heterologous
431 expression of SbtA and SbtB proteins for binding studies. The HCO_3^- uptake deficient cell line
432 *Synechococcus* ΔCS was derived from wild-type *Synechococcus elongatus* PCC7942 by sequential
433 insertional inactivation of the only two endogenous bicarbonate transporters, BCT1 (*cmpABCD* operon)
434 and SbtA (*sbtAB* operon). BCT1 expression was eliminated by replacement of the *cmpA* (IMG ID:
435 637799921, Synpcc7942_1488) and part of the *cmpB* (IMG ID: 637799922, Synpcc7942_1489) genes
436 with a selective kanamycin resistance (kan^R) cassette (Omata et al., 1990). To this end, a 2.5 kb
437 genomic DNA fragment spanning the *cmpA* and *cmpB* genes was amplified by PCR. The kan^R marker
438 was inserted into the central *Bgl*II site of the *cmpAB* fragment, generating gene-specific 3' and 5'
439 flanking sequences for homologous recombination (**Table 1**) and ligated into pUC18 (pUC18::Δ*cmpAB*)
440 which is a non-replicating vector in cyanobacteria. The pUC18::Δ*cmpAB* plasmid was transformed into
441 wild-type and generated the single deletion mutant (ΔC). For the second deletion (ΔS), the full length
442 *sbtA* (IMG ID: 637799907, Synpcc7942_1475) and *sbtB* (IMG ID: 637799908, Synpcc7942_1476) operon
443 was replaced with a chloramphenicol resistance (cm^R) marker gene (Dzelzkalns et al., 1984) in
444 *Synechococcus* ΔC. Two 1100 and 1400 bp genomic DNA fragments up- and downstream of the *sbtAB*
445 operon, respectively, were amplified by PCR (**Table 1**), attached as 3' and 5' genomic flanking sequence
446 to the cm^R marker gene and inserted into plasmid pUC18 (pUC18::Δ*sbtAB*), which was then
447 transformed into *Synechococcus* ΔC to generate the double deletion strain (ΔCS). Cyanobacterial
448 transformation was carried out by natural DNA uptake as described previously (Golden and Sherman,
449 1984). Single cell-derived kan^R and/or cm^R colonies were selected on the appropriate antibiotic-
450 containing media (kanamycin 100 μg ml^{-1}, chloramphenicol 8 μg ml^{-1}) until ΔC and ΔS deletions had

451 fully segregated, which was verified by PCR using primer pairs Cmp-F/Cmp-R and SbtA-F/SbtB-R,
452 respectively (**Table 1**).
453 For protein expression, *sbtA* and *sbtB* genes from *Synechococcus elongatus* PCC7942 and *Cyanobium*
454 *sp.* PCC7001 (IMG ID: 647590134, CPCC7001_1784 and IMG ID: 647590133, CPCC7001_1671,
455 respectively) were synthesized (GenScript, New Jersey, USA) and inserted into the *Sac*I/*Xba*I restriction
456 sites of plasmids pSE2-1 and pSE4-1 which both carry a spectinomycin resistance (sp^R) marker gene
457 (Price et al., 2004; Du et al., 2014) and contain origins of replications for maintenance in *E. coli* and in
458 *Synechococcus elongatus*. Genes of interest were expressed from pSE2-1 under control of the
459 isopropyl β-D-1-thiogalactopyranoside (IPTG)-inducible *lacZ* promoter and *lacIQ* repressor and from
460 pSE4-1 using their native *sbtA* and *sbtB* promoters. The SbtB proteins were C-terminally tagged with a
461 HA epitope (YPYDVPDYA) for immunodetection and 5 or 6 His residues for affinity purification in IMAC
462 assays. For expression of SbtA alone, the appropriate *sbtB* genes were removed by restriction digestion
463 and re-ligation from the *sbtAB* gene inserts in pSE2-1 and pSE4-1. Transformed *E. coli* and
464 cyanobacterial cells were selected on solid media containing 100 and 10 µg ml^{-1} spectinomycin,
465 respectively. Cell lines and expression vectors used in this study are listed in **Table 2**.
466

467 **Growth of *E. coli* and cyanobacteria**

468 For maintenance, mutant selection and protein expression, *E. coli* DH5α derived cell lines were
469 grown at 37 °C in Lysogeny broth (LB) supplemented with 100 µg ml^{-1} spectinomycin as described
470 previously (Du et al., 2014), and expression of SbtA and SbtB proteins was induced for 3 h with 1 mM
471 IPTG. *Synechococcus* ΔCS cell lines were grown at 30 °C in modified BG-11 medium (buffered with 20
472 mM HEPES-KOH pH 8.0 (Maeda et al., 2002; Woodger et al., 2003) in high Ci (2-4% (v/v) CO_2 enriched
473 air) or low Ci (ambient air, 400 ppm CO_2) under constant light (70 µmol m^{-2} s^{-1}). Antibiotics were
474 supplied as appropriate (100 µg ml^{-1} kanamycin, 8 µg ml^{-1} chloramphenicol, 100 µg ml^{-1}
475 spectinomycin). Protein expression of SbtA and SbtB was induced by exposing high Ci-grown
476 cyanobacterial cultures for 4 h to low Ci. For growth assays, dilution series of low Ci-induced cultures
477 grown to mid-log phase were adjusted to OD_{730} of 0.2 and a dilution series spotted onto agar plates
478 containing growth medium with antibiotic supplements. Plates were then incubated in air under 50
479 µmol m^{-2} s^{-1} white light (photoperiod, 12 h light : 12 h dark) for 10 days. Final biomass accumulation
480 was recorded as scanned images.
481

482 **Extraction of native proteins**

483 The method for the isolation of membrane-enriched fractions of native proteins from *E. coli* and
484 *Synechococcus* ΔCS was adapted from previous work (Du et al., 2014). After induction of protein

485 expression, cultures of *E. coli* or S *Synechococcus* ΔCS were harvested in mid-log phase by
486 centrifugation (5 min, 6000 *g*, 23 °C). Cell pellets were washed once with HEPES lysis buffer (50 mM
487 HEPES, 100 mM NaCl, 5% (v/v) glycerol) and treated with 300 U/µl r-Lysozyme (Sigma, USA) for 15 min
488 at 23 °C. Cells were broken with 0.1 mm Zirconia-silica beads (Biospec Products) in a mini-beadbeater
489 16 (Biospec Products) at 3450 oscillations min^{-1} for 6 min in HEPES IMAC binding buffer (50 mM HEPES,
490 100 mM NaCl, 25 mM imidazole, pH 8.0) and 0.1% (v/v) protease inhibitor cocktail (Sigma, USA) and
491 centrifuged for 30 s at 16000 *g* to precipitate cell debris and beads at room temperature. The
492 supernatant was then centrifuged (15 min, 16000 *g*, 4 °C) to pellet the membrane-enriched fraction.
493 Membrane proteins were solubilized in IMAC HEPES binding buffer (50 mM HEPES, 100 mM NaCl, 25
494 M imidazole, pH 8.0) supplemented with 1% (w/v) *n*-dodecyl β-D-maltoside (DDM) by gentle agitation
495 on a rotator for 30 min at 23 °C, and insoluble matter precipitated by centrifugation (5 min, 16000 *g*, 4
496 °C) prior to further analysis.
497

498 **Immobilized metal affinity chromatography (IMAC) protein binding assays**

499 The association of SbtA and HAHis-tagged SbtB proteins was analysed in IMAC binding assays
500 adapted from previous work (Du et al., 2014). Native protein extracts from *E.coli* or *Synechococcus* ΔCS
501 were incubated in IMAC HEPES binding buffer supplemented with potential effector molecules and Ni-
502 charged iminodiacetic acid Profinity™ IMAC Resin (Bio-Rad, USA) on a low speed rotator for 1 h at 23
503 °C. This allowed the His-tag on SbtB to bind to the resin and SbtA to associate with the immobilized
504 SbtB protein. The resin had been prewashed three times with IMAC HEPES binding buffer, and one
505 volume of resin was added to four volumes of the reaction mixture. Depending on the experiment,
506 varying concentrations of $MgCl_2$, $CaCl_2$, $NaHCO_3$, Na_2HPO_4, RUBP, 3PGA, 2OG, ATP, ADP, AMP and
507 cAMP were added to the protein extract-resin mixture as potential effector molecules. Standard
508 binding assays were performed with 200 nM $CaCl_2$ unless stated otherwise. Further details on effector
509 molecules and adenylnucleotide ratios are provided in the figures and captions. The reaction mixture
510 was transferred onto columns, washed with five volumes IMAC HEPES binding buffer by gravity flow
511 through, which removed unbound protein and effector molecules. SbtB was then eluted from the resin
512 with IMAC HEPES elution buffer (50 mM HEPES, 300 mM NaCl, 250 mM imidazole, pH 8.0). The eluted
513 fraction contained the proportion of SbtB protein immobilized on the beads and the amount of SbtA
514 protein retained due to binding to SbtB. IMAC purified SbtA:SbtB complexes were subjected to
515 immunoblot analysis.
516

517 **Immunodetection of SbtA and SbtB proteins and quantification of SbtA:SbtB binding**

518 Aliquots of membrane-enriched and eluted IMAC fractions were supplemented with 2.5% (v/v) β-
519 mercaptoethanol and sample loading buffer (62.5 mM Tris pH 8.0, 2% SDS, 10% glycerol, 0.02% (w/v)

520 Coomassie G250, 0.0025% (w/v) Phenol red), heated for 3 min at 80 °C, centrifuged (30 s, 12000 *g*, 23
521 °C) and separated on linear gradient 4-12% Bis-Tris polyacrylamide gels (NuPAGE® Novex®, Invitrogen,
522 USA) in MES running buffer (50 mM MES, 50 mM Tris base, 0.2% SDS, 1 mM EDTA free acid). Proteins
523 were transferred onto 0.45 µm PVDF (polyvinylidene fluoride) membrane using a semi-dry blotter (Bio-
524 Rad, USA) and Tris-Glycine transfer buffer (48 mM Tris base, 38 mM glycine, 0.038% SDS, 20%
525 methanol). Immunological detection was performed in Tris-Saline buffer (20 mM Tris, 137 mM NaCl,
526 0.1% Tween 20, pH 7.5) with 5% (w/v) skim milk powder as blocking reagent. SbtA protein was
527 detected with a polyclonal antibody generated against a conserved 14 amino acid-epitope (Agrisera,
528 Sweden). The HAHis-tagged SbtB proteins were detected with monoclonal antibodies against the HA-
529 epitope (Sigma, USA). Secondary, alkaline phosphatase-conjugated antibodies (Bio-Rad, USA) were
530 used for fluorometric detection of the immune-reactive bands with the AttoPhos system (Promega,
531 USA). The fluorescence signal was visualized with a ChemiDoc™ MP imaging system (Biorad, USA). The
532 relative signal intensities were quantified based on global background-corrected pixel volumes using
533 ImageLab software (Bio-Rad, USA). Amounts of SbtA protein retained in complexes by binding to SbtB
534 (pixel volumes; y) were plotted against adenylnucleotide ratios (AR; x), using OriginPro v2020 software
535 (OriginLab Corp., USA). The non-linear correlation was fitted by a type 1 sigmoidal-logistic function
536 ($F(x) = y = A/(1 + e^{-k*(x-xc)})$), with A as maximum amount of SbtA bound, *k* as rate (binding) coefficient,
537 and xc as the AR at the inflection point. The adenylnucleotide ratios corresponding to 50% (AR_{50}) and
538 10% (AR_{10}) of SbtA bound to SbtB were estimated from the sigmoidal logistic fitted curves normalized
539 to residual SbtA detected at AR=1.
540

541 **Photosynthetic analysis by membrane inlet mass spectrometry (MIMS) measurements**

542 Net photosynthetic O_2 evolution and Ci uptake rates were calculated from changes in the
543 concentrations of dissolved CO_2 and O_2 in aqueous cyanobacterial cell suspensions measured in a
544 closed custom-built, temperature-controlled cuvette attached to a mass spectrometer (Isoprime IRMS
545 series, Micromass, UK) as described previously (Badger and Andrews, 1982; Badger et al., 1985; Price
546 et al., 2004). The inside of cuvette was separated from the inlet to the mass spectrometer by a gas
547 permeable membrane. Low Ci-induced cell cultures were harvested by centrifugation (4 min, 4000 *g*,
548 23 °C), washed once with CO_2-free BTP (1,3-bis[tris(hydroxymethyl)methylamino]propane) assay buffer
549 (20 mM BTP buffered modified Bg-11(-NO_3), 20 mM NaCl, pH 8.0), and resuspended at cell densities
550 equal to 4 µg ml^{-1} Chl*a*. Chl*a* content was determined spectrophotometrically in 90% (v/v) methanol
551 extracts (Porra et al., 1989). Measurements were performed at 30 °C which is equivalent to the growth
552 temperature for cell cultures. During MIMS measurements, CO_2 uptake was inhibited with 500 µM
553 ethoxyzolamide (EZ). Steady state photosynthetic O_2 evolution in response to light intensity was
554 recorded for cell suspension cultures equilibrated with 1 mM HCO_3^- which constitutes > 98% of the

555 available Ci at pH 8. Illumination (KL1500 HAL light source, Schott, Germany) was increased stepwise
556 from 0 to 15, 50, 200, 490, 850 and 1100 µmol photons m^{-2} s^{-1}. Respiration rates were estimated from
557 O_2 consumption in the dark. Prior to MIMS measurements of Ci response curves, cell cultures were
558 depleted for Ci by bubbling with N_2 in white light (400 µmol m^{-2} s^{-1}) for at least 10 min and
559 photosynthetic O_2 evolution rates recorded following incremental additions of bicarbonate. Steady
560 state O_2 evolution rates (*V*) normalized to Chl*a* contents were plotted against Ci substrate (S)
561 concentrations, and resulting curves were fitted by the Michaelis-Menten equation, $V = (V_{max}\ [S])/(k_{0.5}$
562 $+ [S]$, using OriginPro v2021 software. Maximum O_2 evolution rates (V_{maxO_2}) were calculated as an
563 approximation for maximum bicarbonate uptake by SbtA. Affinity of SbtA for HCO_3^- was deduced from
564 the Ci concentration supporting half-maximal activity ($k_{0.5Ci}$). Effects of 300 s-illuminations with high
565 (HL, 1400 µmol m^{-2} s^{-1}) and low (LL, 200 µmol m^{-2} s^{-1}) white light on HCO_3^-uptake and steady state O_2
566 evolution rates were determined in cell cultures that had been equilibrated in the dark after addition
567 of aqueous $NaHCO_3$ solution to a final concentration of 250 or 500 µM.
568

569 **Ci uptake measurement by silicon oil centrifugation-filtration**

570 Light- and dark stimulated uptake of active species of $[^{14}C]HCO_3^-$ in cyanobacterial cell cultures
571 was measured using the silicon oil centrifugation-filtration method as described previously (Kaplan et
572 al., 1980; Price and Badger, 1989). Low Ci-induced cell cultures were prepared as described for MIMS
573 analyses. Cells were pelleted by centrifugation (4 min, 4000 *g*, 23 °C) and resuspended in CO_2-free BTP
574 at pH 8 or pH 9 at densities equal to 4 µg ml^{-1} Chl*a*. Ci uptake was determined in 200 µl aliquots of cells
575 supplemented with 500 µM EZ that were transferred into translucent centrifuge tubes on top of a
576 silicon oil layer (mixture of AR200 : AR20 3.5 : 4 (v/v)) which separated the cells from the kill solution
577 (50% methanol, 2 N NaOH) in the bottom of the tube. For low light (30 µmol photons m^{-2} s^{-1}) activation
578 experiments, cells were equilibrated with 500 µM $[^{14}C]HCO_3^-$ substrate mix (aqueous $NaHCO_3$ solution
579 spiked with radioactive $[^{14}C]NaHCO_3$, pH 9.5) for 60 s either in the dark (dark control) or after
580 exposure to low light for 30 or 60 s following a transfer from the dark. Uptake was terminated by rapid
581 filtering of the cells into the kill solution during 20 s centrifugation at set maximum speed (microfuge
582 B, Beckman, USA). For dark-inactivation experiments, cell cultures were depleted of Ci in the light (400
583 µmol m^{-2} s^{-1}) prior to initiation of HCO_3^- uptake by adding 500 µM $[^{14}C]HCO_3^-$ substrate mix, either in
584 the light (400 µmol m^{-2} s^{-1}), or at various time points in the dark after cells had been transferred from
585 the light into the dark for 15, 30, 45, 60, 90 and 180 s. Cells were incubated with ^{14}C-labelled substrate
586 for 30 s, and uptake was terminated by 20 s centrifugation. Tubes were immediately frozen in dry ice.
587 The tips containing the cell pellets were cut off, resuspended in 2 N NaOH and mixed with 5 volumes
588 scintillation fluid (Ultima Gold™ XR, PerkinElmer) for ^{14}C-CPM counting in a TRI-CARB liquid scintillation
589 counter (PerkinElmer, USA). Ci uptake rates were calculated based on the specific activity of the

590 [^{14}C]HCO_3^- substrate mix. To test the inhibitory effect of EZ, cells were incubated with varying
591 concentrations of EZ (0, 250, 375, 500, 750, 1000 µM) for 5 min in the light before adding 500 µM
592 [^{14}C]HCO_3^- substrate mix for 30 s-uptake measurements.
593
594 **Bioinformatics**
595 Homologous SbtA and SbtB proteins were identified in BLASTP (Altschul et al., 1990) searches and
596 multiple pairwise amino acid sequence alignments generated in Geneious Prime 2021
597 (https://www.geneious.com) with MUSCLE software (Edgar, 2004). Further details on aligned proteins
598 is given in **Supporting Information Tables S1** and **S2**. The three-dimensional domain homology models
599 of the $SbtB_{7942}$, $SbtA_{7942}$ and $SbtA_{7001}$ monomers were generated using AlphaFold2 (ColabFold v1.5.2:
600 AlphaFold2 using MMseqs2) (Mirdita et al., 2022). Three-dimensional structure visualization and
601 comparisons were performed with UCSF Chimera v.1.16 (http://www.cgl.ucsf.edu/chimera) (Meng et
602 al., 2006) and UCSF ChimeraX (https://www.rbvi.ucsf.edu/chimerax) (Pettersen et al., 2021). The
603 overall folds of $SbtB_{7942}$ and $SbtB_{7001}$ chain A with ADP (PDB: 6MMC) or Ca^{2+} and ATP ligands (PDB:
604 6MM2) proteins were compared by superposition onto each other and the cryo-EM structure of
605 $SbtB_{6803}$ (PDB: 7EGK, chains B, D, or F). The $SbtA_{7942}$ and $SbtA_{7001}$ homology models were compared by
606 superposition onto each other and the cryo-EM structure of $SbtA_{6803}$ (PDB: 7EGK, chains A, C or E).
607
608 **Statistics**
609 Statistically significant differences between data sets were determined by performing a one-way
610 analysis of variance (ANOVA) and post-hoc Tukey's Honest Significant Difference (HSD) test (Tukey,
611 1949), using a type I error level α=0.05 (P=0.05) as threshold.
612
613 **Acknowledgements**
614 This work was supported by the Australian Government through the Australian Research Council
615 Centre of Excellence for Translational Photosynthesis (CE1401000015). Molecular graphics and
616 analyses were performed with UCSF ChimeraX, developed by the Resource for Biocomputing,
617 Visualization, and Informatics at the University of California, San Francisco, with support from National
618 Institutes of Health R01-GM129325 and the Office of Cyber Infrastructure and Computational Biology,
619 National Institute of Allergy and Infectious Diseases.
620
621 **Author Contributions**
622 BF, BM and GDP: Conceptualization and Methodology. BF, BM and LR: Investigation. BF: Formal data
623 analysis. BF: Writing - original manuscript draft. All authors: Writing- review & editing. GDP: Funding
624 acquisition.
625
626 **Conflict of Interest**
627 No conflicts of interest are declared.
628
629

Data availability

All data supporting this study are available within the main manuscript and the supplementary information published online. Any data not shown are available from the corresponding author upon request.

References

Agostoni M, Montgomery BL (2014) Survival strategies in the aquatic and terrestrial world: The impact of second messengers on cyanobacterial processes. Life **4:** 745-769

Altschul SF, Gish W, Miller W, Myers EW, Lipman DJ (1990) Basic local alignment search tool. Journal of Molecular Biology **215:** 403-410

Angeleri M, Muth-Pawlak D, Aro E-M, Battchikova N (2016) Study of O-phosphorylation sites in proteins involved in photosynthesis-related processes in *Synechocystis sp.* strain PCC 6803: application of the SRM approach. Journal of Proteome Research **15:** 4638–4652

Atkinson DE, Walton GM (1967) Adenosine triphosphate conservation in metabolic regulation: Rat liver citrate cleavage enzyme. Journal of Biological Chemistry **242:** 3239-3241

Badger MR, Andrews TJ (1982) Photosynthesis and inorganic carbon usage by the marine cyanobacterium, *Synechococcus sp*. Plant Physiology **70:** 517-523

Badger MR, Bassett M, Comins HN (1985) A model for HCO_3^- accumulation and photosynthesis in the cyanobacterium *Synechococcus sp*: Theoretical predictions and experimental observations. Plant Physiology **77:** 465-471

Badger MR, Price GD (1992) The CO_2 concentrating mechanism in cyanobactiria and microalgae. Physiologia Plantarum **84:** 606-615

Bornefeld T, Simonis W (1974) Effects of light, temperature, pH, and inhibitors on the ATP level of the blue-green alga *Anacystic nidulans*. Planta **115:** 309-318

Cann M (2004) Bicarbonate stimulated adenylyl cyclases. IUBMB Life **56:** 529-534

Chapman AG, Fall L, Atkinson DE (1971) Adenylate energy charge in *Escherichia coli* during growth and starvation. Journal of Bacteriology **108:** 1072-1086

De la Fuente IM, Cortés JM, Valero E, Desroches M, Rodrigues S, Malaina I, Martínez L (2014) On the dynamics of the adenylate energy system: homeorhesis vs homeostasis. PLOS ONE **9:** e108676

Du J, Förster B, Rourke L, Howitt SM, Price GD (2014) Characterisation of cyanobacterial bicarbonate transporters in *E. Coli* shows that SbtA homologs are functional in this heterologous expression system. PLoS ONE **9:** e115905

Dzelzkalns VA, Owens GC, Bogorad L (1984) Chloroplast promoter driven expression of the chloramphenicol acetyl transferase gene in a cyanobacterium. Nucleic acids research **12:** 8917-8925

Edgar RC (2004) MUSCLE: a multiple sequence alignment method with reduced time and space complexity. BMC Bioinformatics **5:** 113

Espie G, Kimber M (2011) Carboxysomes: cyanobacterial RubisCO comes in small packages. Photosynthesis Research **109:** 7-20

Fang S, Huang X, Zhang X, Zhang M, Hao Y, Guo H, Liu L-N, Yu F, Zhang P (2021) Molecular mechanism underlying transport and allosteric inhibition of bicarbonate transporter SbtA. Proceedings of the National Academy of Sciences **118:** e2101632118

Field CB, Behrenfeld MJ, Randerson JT, Falkowski P (1998) Primary production of the biosphere: Integrating terrestrial and oceanic components. Science **281:** 237-240

Forchhammer K, Lüddecke J (2016) Sensory properties of the PII signalling protein family. The FEBS Journal **283:** 425-437

Forchhammer K, Selim KA (2020) Carbon/nitrogen homeostasis control in cyanobacteria. FEMS Microbiology Reviews **44:** 33-53

Golden SS, Sherman LA (1984) Optimal conditions for genetic transformation of the cyanobacterium Anacystis nidulans R2. Journal of Bacteriology **158:** 36-42

Hammer A, Hodgson DRW, Cann MJ (2006) Regulation of prokaryotic adenylyl cyclases by CO2. The Biochemical Journal **396:** 215-218

Huergo LF, Chandra G, Merrick M (2013) PII signal transduction proteins: nitrogen regulation and beyond. FEMS Microbiology Reviews **37:** 251-283

Huergo LF, Dixon R (2015) The emergence of 2-oxoglutarate as a master regulator metabolite. Microbiology and Molecular Biology Reviews **79:** 419-435

Kaczmarski JA, Hong N-S, Mukherjee B, Wey LT, Rourke L, Förster B, Peat TS, Price GD, Jackson CJ (2019) Structural basis for the allosteric regulation of the SbtA bicarbonate transporter by the PII-like protein, SbtB, from *Cyanobium sp.* PCC7001. Biochemistry **58:** 5030-5039

Kallas T, Castenholz RW (1982) Internal pH and ATP-ADP pools in the cyanobacterium *Synechococcus sp.* during exposure to growth-inhibiting low pH. Journal of Bacteriology **149:** 229-236

Kaplan A, Badger M, Berry J (1980) Photosynthesis and the intracellular inorganic carbon pool in the bluegreen alga *Anabaena variabilis*: Response to external CO_2 concentration. Planta **149:** 219-226

Kaplan A, Reinhold L (1999) CO_2 concentrating mechanisms in photosynthetic microorganisms. Annual Review of Plant Physiology and Plant Molecular Biology **50:** 539-570

Kaplan A, Zenvirth D, Marcus Y, Omata T, Ogawa T (1987) Energization and activation of inorganic carbon uptake by light in cyanobacteria. Plant Physiology **84:** 210-213

Leganés F, Forchhammer K, Fernández-Piñas F (2009) Role of calcium in acclimation of the cyanobacterium *Synechococcus elongatus* PCC 7942 to nitrogen starvation. Microbiology **155:** 25-34

Liu H, Nolla H, Campbell L (1997) Prochlorococcus growth rate and contribution to primary production in the equatorial and subtropical North Pacific Ocean. Aquatic Microbial Ecology **12:** 39-47

Liu X-Y, Hou W-T, Wang L, Li B, Chen Y, Chen Y, Jiang Y-L, Zhou C-Z (2021) Structures of cyanobacterial bicarbonate transporter SbtA and its complex with PII-like SbtB. Cell Discovery **7:** 63

Long BM, Rae BD, Rolland V, Förster B, Price GD (2016) Cyanobacterial CO_2-concentrating mechanism components: function and prospects for plant metabolic engineering. Current Opinion in Plant Biology **31:** 1-8

Maeda S-i, Badger MR, Price GD (2002) Novel gene products associated with NdhD3/D4-containing NDH-1 complexes are involved in photosynthetic CO_2 hydration in the cyanobacterium, *Synechococcus sp.* PCC7942. Molecular Microbiology **43:** 425-435

McGinn PJ, Price GD, Maleszka R, Badger MR (2003) Inorganic carbon limitation and light control the expression of transcripts related to the CO_2-concentrating mechanism in the cyanobacterium *Synechocystis sp.* strain PCC6803. Plant Physiology **132:** 218-229

McGrath JM, Long SP (2014) Can the cyanobacterial carbon-concentrating mechanism increase photosynthesis in crop species? A theoretical analysis. Plant Physiology **164:** 2247-2261

Meng EC, Pettersen EF, Couch GS, Huang CC, Ferrin TE (2006) Tools for integrated sequence-structure analysis with UCSF Chimera. BMC Bioinformatics **7:** 339-339

Meyer MT, McCormick AJ, Griffiths H (2016) Will an algal CO_2-concentrating mechanism work in higher plants? Current Opinion in Plant Biology **31:** 181-188

Mirdita M, Schütze K, Moriwaki Y, Heo L, Ovchinnikov S, Steinegger M (2022) ColabFold: making protein folding accessible to all. Nature Methods **19:** 679-682

Ogawa T, Miyano A, Inoue Y (1985) Photosystem-I-driven inorganic carbon transport in the cyanobacterium, Anacystis nidulans. Biochimica et Biophysica Acta (BBA) - Bioenergetics **808:** 77-84

Ohkawa H, Sonoda M, Hagino N, Shibata M, Pakrasi HB, Ogawa T (2002) Functionally distinct NAD(P)H dehydrogenases and their membrane localization in *Synechocystis sp*. PCC6803. Functional Plant Biology **29:** 195-200

Ohmori M, Okamoto S (2004) Photoresponsive cAMP signal transduction in cyanobacteria. Photochemical & Photobiological Sciences **3:** 503-511

Omata T, Carlson TJ, Ogawa T, Pierce J (1990) Sequencing and Modification of the Gene Encoding the 42-Kilodalton Protein in the Cytoplasmic Membrane of Synechococcus PCC 7942. Plant physiology **93:** 305-311

Omata T, Price GD, Badger MR, Okamura M, Gohta S, Ogawa T (1999) Identification of an ATP-binding cassette transporter involved in bicarbonate uptake in the cyanobacterium *Synechococcus sp.* strain PCC 7942. Proceedings of the National Academy of Sciences **96:** 13571-13576

Oren N, Timm S, Frank M, Mantovani O, Murik O, Hagemann M (2021) Red/far-red light signals regulate the activity of the carbon-concentrating mechanism in cyanobacteria. Science Advances **7:** eabg0435

Pettersen EF, Goddard TD, Huang CC, Meng EC, Couch GS, Croll TI, Morris JH, Ferrin TE (2021) UCSF ChimeraX: Structure visualization for researchers, educators, and developers. Protein Sci **30:** 70-82

Porra RJ, Thompson WA, Kriedemann PE (1989) Determination of accurate extinction coefficients and simultaneous equations for assaying chlorophylls a and b extracted with four different solvents: verification of the concentration of chlorophyll standards by atomic absorption spectroscopy. Biochimica et Biophysica Acta (BBA) - Bioenergetics **975:** 384-394

Price G (2011) Inorganic carbon transporters of the cyanobacterial CO_2 concentrating mechanism. Photosynthesis Research **109:** 47-57

Price GD, Badger MR (1989) Ethoxyzolamide inhibition of CO_2 uptake in the cyanobacterium *Synechococcus* PCC7942 without apparent inhibition of internal carbonic anhydrase activity. Plant Physiology **89:** 37-43

Price GD, Badger MR (1989) Isolation and characterization of high CO_2-requiring-mutants of the cyanobacterium *Synechococcus* PCC7942: Two phenotypes that accumulate inorganic carbon but are apparently unable to generate CO_2 within the carboxysome. Plant Physiology **91:** 514-525

Price GD, Badger MR, Woodger FJ, Long BM (2008) Advances in understanding the cyanobacterial CO_2-concentrating-mechanism (CCM): functional components, Ci transporters, diversity, genetic regulation and prospects for engineering into plants. Journal of Experimental Botany **59:** 1441-1461

Price GD, Pengelly JJL, Förster B, Du J, Whitney SM, von Caemmerer S, Badger MR, Howitt SM, Evans JR (2013) The cyanobacterial CCM as a source of genes for improving photosynthetic CO_2 fixation in crop species. Journal of Experimental Botany **64:** 753-768

Price GD, Shelden MC, Howitt SM (2011) Membrane topology of the cyanobacterial bicarbonate transporter, SbtA, and identification of potential regulatory loops. Molecular Membrane Biology **28:** 265-275

Price GD, Woodger FJ, Badger MR, Howitt SM, Tucker L (2004) Identification of a SulP-type bicarbonate transporter in marine cyanobacteria. Proceedings of the National Academy of Sciences **101:** 18228-18233

Radchenko MV, Thornton J, Merrick M (2010) Control of AmtB-GlnK complex formation by intracellular levels of ATP, ADP, and 2-oxoglutarate. Journal of Biological Chemistry **285:** 31037-31045

Radchenko MV, Thornton J, Merrick M (2013) P_{II} signal transduction proteins are ATPases whose activity is regulated by 2-oxoglutarate. Proceedings of the National Academy of Sciences **110:** 12948-12953

Rae BD, Förster B, Badger MR, Price GD (2011) The CO_2-concentrating mechanism of *Synechococcus* WH5701 is composed of native and horizontally-acquired components. Photosynthesis Research **109:** 59-72

Rath A, Glibowicka M, Nadeau VG, Chen G, Deber CM (2009) Detergent binding explains anomalous SDS-PAGE migration of membrane proteins. Proceedings of the National Academy of Sciences **106:** 1760-1765

Rust MJ, Golden SS, O'Shea EK (2011) Light-driven changes in energy metabolism directly entrain the cyanobacterial circadian oscillator. Science **331:** 220-223

Sánchez-Baracaldo P, Bianchini G, Di Cesare A, Callieri C, Chrismas NAM (2019) Insights into the evolution of picocyanobacteria and phycoerythrin genes (*mpeBA* and *cpeBA*). Frontiers in Microbiology **10:** 45

Schwarz D, Nodop A, Hüge J, Purfürst S, Forchhammer K, Michel K-P, Bauwe H, Kopka J, Hagemann M (2011) Metabolic and transcriptomic phenotyping of inorganic carbon acclimation in the cyanobacterium *Synechococcus elongatus* PCC 7942. Plant Physiology **155:** 1640-1655

Selim KA, Haase F, Hartmann MD, Hagemann M, Forchhammer K (2018) P_{II}-like signaling protein SbtB links cAMP sensing with cyanobacterial inorganic carbon response. Proceedings of the National Academy of Sciences **115:** E4861-E4869

Selim KA, Haffner M, Burkhardt M, Mantovani O, Neumann N, Albrecht R, Seifert R, Krüger L, Stülke J, Hartmann MD, Hagemann M, Forchhammer K (2021) Diurnal metabolic control in cyanobacteria requires perception of second messenger signaling molecule c-di-AMP by the carbon control protein SbtB. Science Advances **7:** eabk0568

Selim KA, Haffner M, Mantovani O, Albrecht R, Zhu H, Hagemann M, Forchhammer K, Hartmann MD (2023) Carbon signaling protein SbtB possesses atypical redox-regulated apyrase activity to facilitate regulation of bicarbonate transporter SbtA. Proceedings of the National Academy of Sciences **120:** e2205882120

Selim KA, Haffner M, Watzer B, Forchhammer K (2019) Tuning the in vitro sensing and signaling properties of cyanobacterial PII protein by mutation of key residues. Scientific Reports **9:** 18985

Shibata M, Katoh H, Sonoda M, Ohkawa H, Shimoyama M, Fukuzawa H, Kaplan A, Ogawa T (2002) Genes essential to sodium-dependent bicarbonate transport in cyanobacteria. Journal of Biological Chemistry **277:** 18658-18664

Spät P, Maček B, Forchhammer K (2015) Phosphoproteome of the cyanobacterium Synechocystis sp. PCC 6803 and its dynamics during nitrogen starvation. Frontiers in Microbiology **6**

Sültemeyer D, Klughammer B, Badger MR, Dean Price G (1998) Fast induction of high-affinity HCO_3^- transport in cyanobacteria. Plant Physiology **116:** 183-192

Takano S, Tomita J, Sonoike K, Iwasaki H (2015) The initiation of nocturnal dormancy in Synechococcus as an active process. BMC Biology **13:** 36

Tamoi M, Miyazaki T, Fukamizo T, Shigeoka S (2005) The Calvin cycle in cyanobacteria is regulated by CP12 via the NAD(H)/NADP(H) ratio under light/dark conditions. The Plant Journal **42:** 504-513

797 **Thauer RK, Jungermann K, Decker K** (1977) Energy conservation in chemotrophic anaerobic bacteria.
798 Bacteriological Reviews **41:** 100-180
799 **Torrecilla I, Leganés F, Bonilla I, Fernández-Piñas F** (2004) Light-to-dark transitions trigger a transient increase in
800 intracellular Ca^{2+} modulated by the redox state of the photosynthetic electron transport chain in the
801 cyanobacterium *Anabaena sp.* PCC7120. Plant, Cell & Environment **27:** 810-819
802 **Tukey JW** (1949) Comparing individual means in the analysis of variance. Biometrics **5:** 99-114
803 **Wheatley NM, Eden KD, Ngo J, Rosinski JS, Sawaya MR, Cascio D, Collazo M, Hoveida H, Hubbell WL, Yeates TO**
804 (2016) A PII-like protein regulated by bicarbonate: Structural and biochemical studies of the
805 carboxysome-associated CPII protein. Journal of Molecular Biology **428:** 4013-4030
806 **Woodger FJ, Badger MR, Price GD** (2003) Inorganic carbon limitation induces transcripts encoding components
807 of the CO_2-concentrating mechanism in *Synechococcus sp.* PCC7942 through a redox-independent
808 pathway. Plant Physiology **133:** 2069-2080
809 **Xu M, Su Z** (2009) Computational prediction of cAMP receptor protein (CRP) binding sites in cyanobacterial
810 genomes. BMC Genomics **10:** 23
811 **Yaginuma H, Kawai S, Tabata KV, Tomiyama K, Kakizuka A, Komatsuzaki T, Noji H, Imamura H** (2014) Diversity
812 in ATP concentrations in a single bacterial cell population revealed by quantitative single-cell imaging.
813 Scientific reports **4:** 6522-6522
814 **Zeth K, Fokina O, Forchhammer K** (2014) Structural basis and target-specific modulation of ADP sensing by the
815 *Synechococcus elongatus* PII signaling protein. The Journal of Biological Chemistry **289:** 8960-8972

816

Figures and Tables

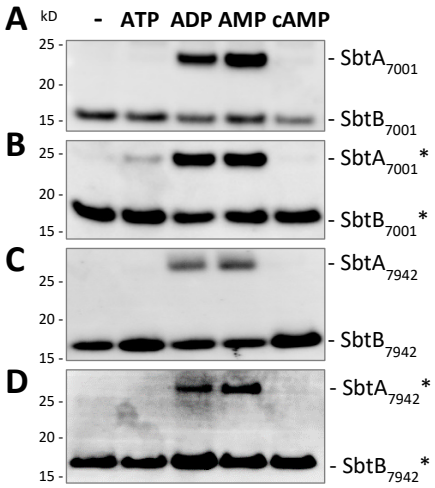

Fig. 1. Association of SbtA and cognate SbtB proteins in response to adenylnucleotides.
The $SbtA_{7001}$- $SbtB_{7001}$ and $SbtA_{7942}$- $SbtB_{7942}$ pairs were expressed in *E. coli* (**A, C**) and *Synechococcus* ΔCS (denoted by *; **B, D**). The HAHis-tagged SbtB proteins were immobilized to examine interaction with SbtA proteins and adenylnucleotides (2 mM ATP, ADP, AMP, or cAMP) during *in vitro* IMAC binding assays. The HAHis-SbtB protein and corresponding amounts of SbtA retained in SbtA:SbtB complexes were detected by immunoblot analyses. Representative results are shown of n=3-8 experiments per adenylnucleotide treatment.

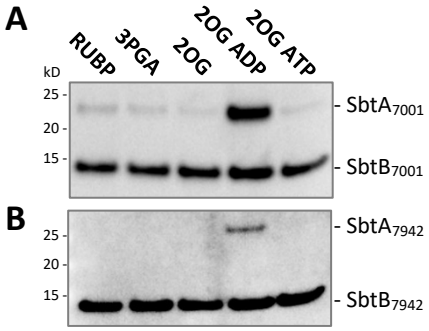

Fig. 2. The association of SbtA and cognate SbtB proteins is not directly linked to key metabolites of the CBB cycle (RUBP, 3PGA) and the TCA cycle (2OG).

In vitro IMAC binding assays were performed with the $SbtA_{7001}$- $SbtB_{7001}$ (**A**) and $SbtA_{7942}$- $SbtB_{7942}$ (**B**) pairs expressed in *E. coli* in the presence of 2 mM RUBP, 3PGA or 2OG, and 2 mM 2OG combined with 2 mM ADP, or ATP (2OG ADP and 2OG ATP, respectively). The representative immunoblot images show HAHis-tagged SbtB proteins and the SbtA proteins retained in SbtA:SbtB complexes; n=2.

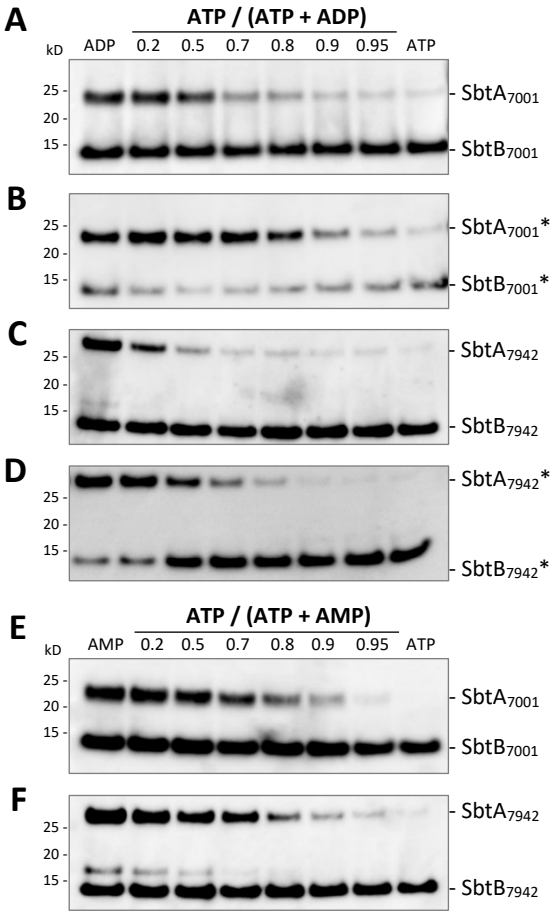

Fig. 3. Effects of ATP:ADP and ATP:AMP ratios on the association of SbtA and SbtB proteins. The $SbtA_{7001}$-$SbtB_{7001}$ (**A, C, E**) and $SbtA_{7942}$-$SbtB_{7942}$ (**B, D, F**) pairs were expressed in *E. coli* (**A, C, E, F**) and in *Synechococcus* ΔCS (denoted by *; **B, D**). Variation in energy charge was simulated during *in vitro* IMAC binding assays by different molar ratios of ATP:ADP (**A-D**) and ATP:AMP (**E, F**), with a total adenylnucleotide concentration of 2 mM. Representative immunoblot images of HAHis-tagged SbtB and SbtA proteins retained in SbtA:SbtB complexes of n=3-4 per adenylnucleotide treatment. The 17 kD-protein above $SbtB_{7942}$ is a fragment occasionally detected with the anti-SbtA antibody (**C, F**).

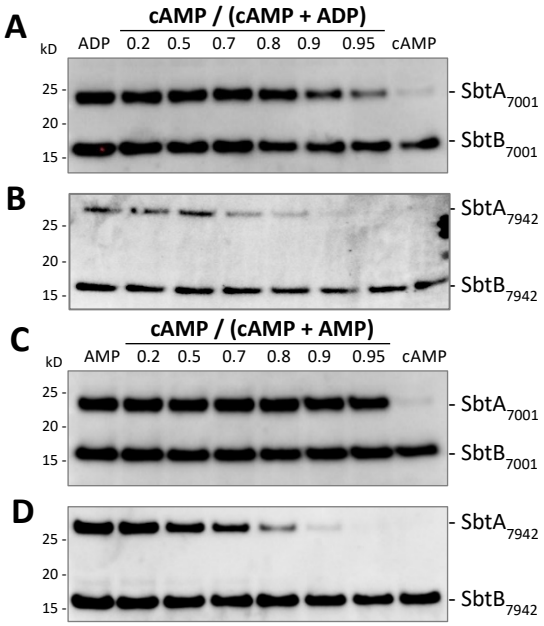

Fig. 4. Effects of the cAMP:ADP and cAMP:AMP ratios on the association of SbtA and SbtB proteins. *In vitro* IMAC binding assays were performed across a range of cAMP:ADP (**A, B**) and cAMP:AMP (**C, D**) ratios, with a total adenylnucleotide concentration of 2 mM. The $SbtA_{7001}$- $SbtB_{7001}$ (**A, C**) and $SbtA_{7942}$- $SbtB_{7942}$ (**B, D**) pairs were expressed in *E. coli*. The immunoblot images show HAHis-tagged SbtB and SbtA proteins retained in SbtA:SbtB complexes and are representative of three independent experiments per adenylnucleotide treatment.

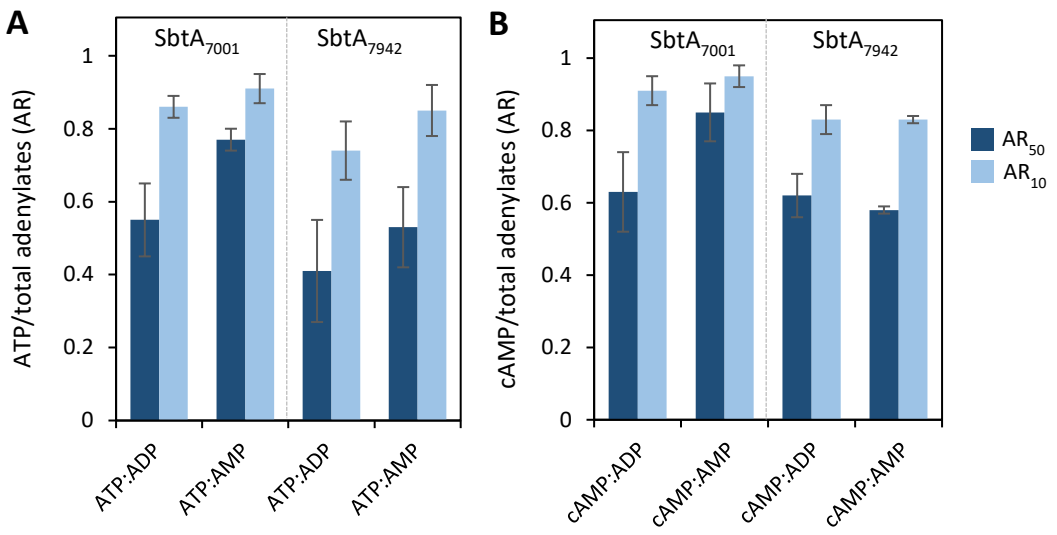

Fig. 5. Quantitative estimates for the association of SbtA and SbtB proteins in response to different adenylnucleotide ratios (AR). The ratios of ATP:ADP or AMP (**A**) and cAMP:ADP or AMP (**B**) that supported 50% (AR_{50}) and 10% (AR_{10}) of SbtA bound to SbtB were estimated from sigmoidal logistic curve fits (Fig. S4). AR values are means (± SE) of 3-4 independent experiments. AR values were not significantly different across each AR category at a *P*=0.05 threshold (AR_{50} *P*=0.232, AR_{10} *P*=0.275).

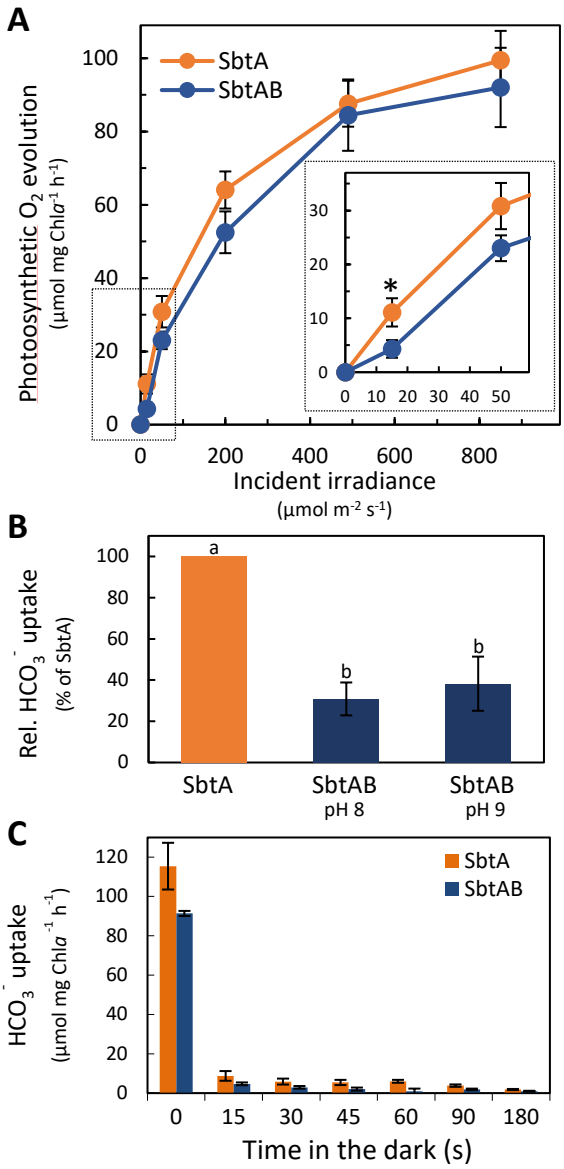

Fig. 6 Light-dependent bicarbonate uptake by SbtA is modulated by SbtB in *Synechococcus* ΔCS. The $SbtA_{7942}$ protein was expressed alone (SbtA) or with $SbtB_{7942}$ (SbtAB) in *Synechococcus* ΔCS (ΔCS) at low Ci in the light. CO_2 uptake was inhibited by EZ to restrict Ci acquisition to bicarbonate uptake by SbtA. (**A**) HCO_3^- uptake-dependent gross photosynthetic O_2 evolution rates in response to stepwise increased light intensity after 1 h dark-adaptation. Respiratory O_2 consumption was the same for SbtA and SbtAB (27 ± 4 and 27 ± 3, respectively). Values are means ± SE; n=4-5. (**B**) Induction of HCO_3^- transport activity of SbtA in dark-adapted cells immediately after dark-to-low light (30 µmol m^{-2} s^{-1}) transitions at pH 8 and pH 9 during 30-60 s pulses of $[^{14}C]HCO_3^-$ uptake, using silicon oil centrifugation-filtration. HCO_3^- uptake rates are shown relative to cells expressing SbtA alone; n=4-5. Relative HCO_3^- uptake rates were calculated by subtraction of the unspecific incorporation of ^{14}C-label, mainly due to extracellular $[^{14}C]$ HCO_3^- in the water shell surrounding each cell and a very small amount of $^{14}CO_2$ diffusion into the cells. This was derived from ^{14}C-label incorporation into Ci uptake inhibited ΔCS (38% ± 6 (pH 8) and 42% ± 8 (pH 9). (**C**) HCO_3^- uptake rates normalized to Chl*a* content at various time points after a light (400 µmol m^{-2} s^{-1}) to dark shift. Values are means ± SE; n=3-5. Statistically significant differences ($P < 0.05$) are denoted by an asterisk (**A**) or different letters (**B**).

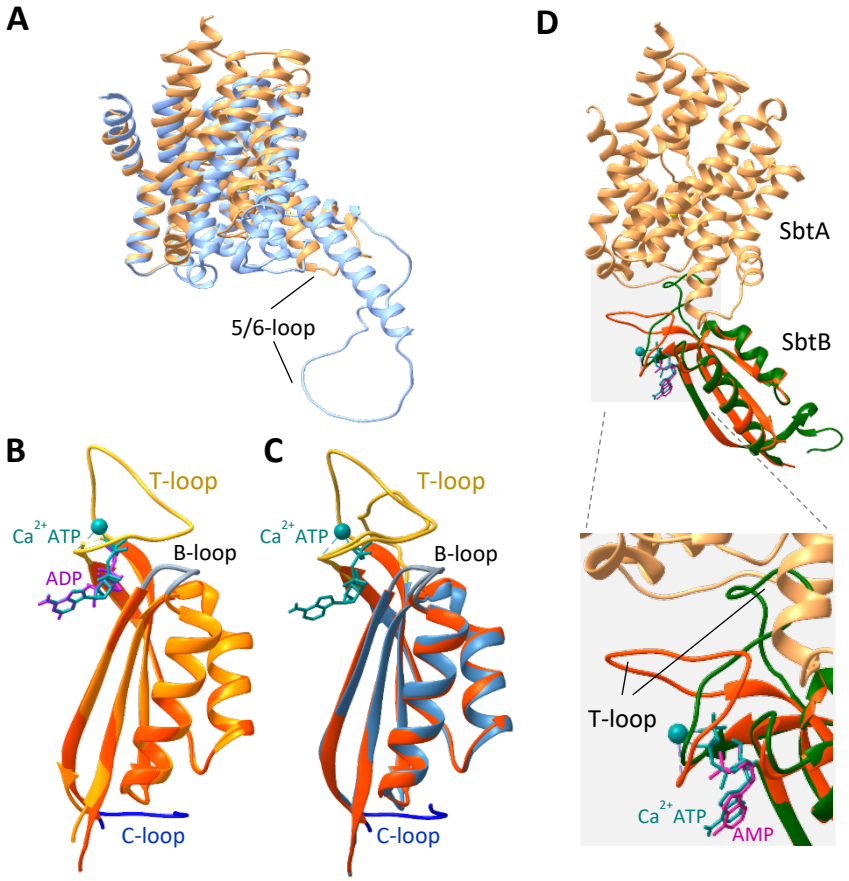

Fig 7. Structural comparison of the overall fold of SbtA and SbtB protein models. (**A**) Superposition of homology models of $SbtA_{7001}$ (light orange) and $SbtA_{7942}$ (light blue). The core domains and arrangement of the transmembrane helices are well matched but the 5/6 loop connecting transmembrane helix 5 and 6 is divergent, protruding further into the cytoplasm on $SbtA_{7942}$. (**B**) Superposition of the three-dimensional models based on crystal structures of $SbtB_{7001}$ with Ca^{2+} and ATP ligands (red-orange, $SbtB_{7001}$-CaATP; PDB: 6MM2) and $SbtB_{7001}$ with ADP bound (orange, $SbtB_{7001}$-ADP; PDB: 6MMC), demonstrating that ligand-induced structural differences affect primarily the T-loop. The T-loop assumes a closed conformation in $SbtB_{7001}$-CaATP and an open, disordered state in $SbtB_{7001}$-ADP which was not resolved in crystals as indicated by the dashed line. (**C**) Superposition the of the homology model of the apo-$SbtB_{7942}$ monomer (blue) on $SbtB_{7001}$-CaATP; both SbtB proteins are predicted to be nearly identical in three-dimensional structures. (**D**) Superposition of the $SbtA_{7001}$ and $SbtB_{7001}$-CaATP onto a $SbtA_{6803}$ monomer (PDB: 7EGK, chain C) associated with a SbtB680-AMP monomer (chain D) which were extracted from the trimeric $SbtAB_{6803}$ cryo-EM structure (PDB: 7EGK). Since the three-dimensional architecture of $SbtA_{7001}$ and $SbtA_{6803}$ are highly similar (Fig. S12), only $SbtA_{7001}$ is shown for clarity. The core structure of $SbtB_{7001}$-CaATP and $SbtB_{6803}$-AMP is nearly identical, but the T-loop conformations diverge in a ligand-specific manner consistent with the observed SbtA:SbtB interaction in this study (enlarged). Binding of AMP to $SbtB_{6803}$ (green) promotes an open T-loop conformation which extends into SbtA consistent with SbtA:SbtB association, whereas Ca^{2+}ATP bound to $SbtB_{7001}$ (red-orange) promotes folding of the T-loop away from SbtA.

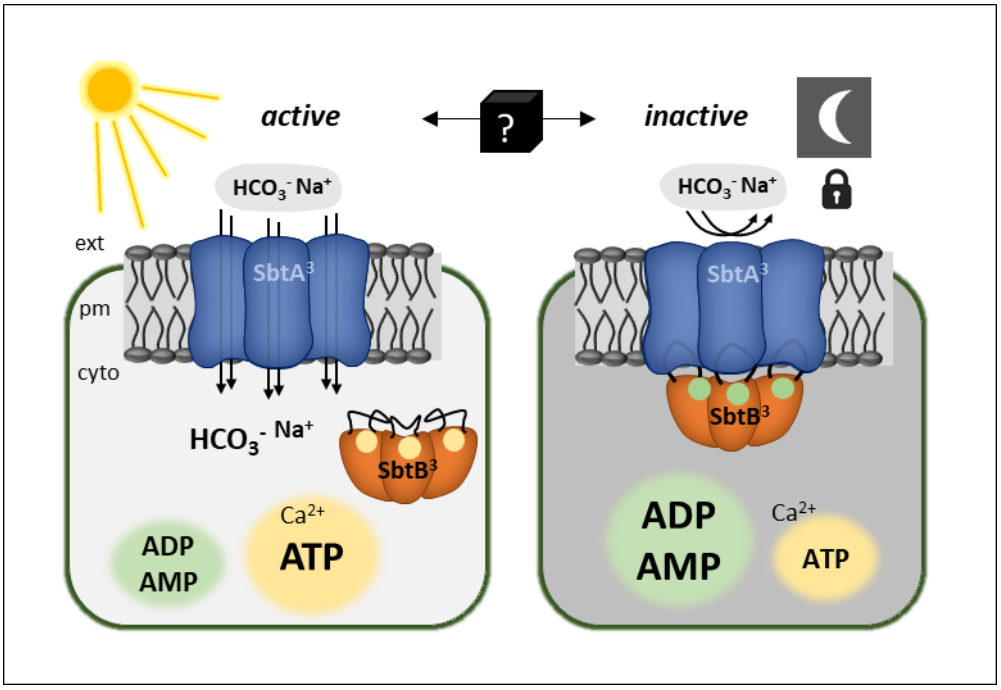

Fig. 8. Proposed model for regulation of SbtA bicarbonate transport activity involving SbtB by environmental stimuli and the adenylate energy charge (AEC). In the light, expression of SbtA and SbtB in *Synechococcus elongatus* is induced by low Ci availability. The plasma membrane (pm)-integral SbtA trimer($SbtA^3$) actively transports bicarbonate from the external environment (ext) into the cytoplasm (cyto) presumably dissociated from SbtB. SbtA activity depends on Na^+- symport and requires a cell-inward-directed Na^+ gradient with a probable HCO_3^-:Na^+ symport stoichiometry of 1:1 through each monomer. Light-stimulated photosynthetic electron transport sustains high levels of intracellular ATP over ADP and AMP, i.e. high AEC, which facilitates binding of Ca^{2+}ATP to SbtB trimers ($SbtB^3$), stabilizing the SbtB T-loops, and SbtB remains dissociated from SbtA. In prolonged darkness, cells operate at a lower AEC. Relatively higher amounts of ADP and AMP replace ATP as ligands in SbtB trimers, which favours open T-loops, and inactive SbtA:SbtB complexes are formed. In such scenario, SbtA reactivation after a transition from dark to light would depend on the rate of increase in AEC and concomitant AEC-dependent dissociation of SbtB.

Table 1. Primers for generation of the bicarbonate transporter-deficient *Synechococcus* ΔCS mutant.

Genes targeted, inactivation plasmid [b]	Primer [a]	Primer sequence 5' -> 3'	Description
cmpA cmpB, pUC18::Δ*cmpAB*	Cmp-F Cmp-R	TTGTCCATCTTTAGAGGCATC TTCAACAGCAACAAATAAACTC	2345 bp genomic fragment spanning *cmpA* and *cmpB*. The *kan*^{R} cassette was inserted into the central *Bgl*II site 3' of *cmpA*.
sbtA sbtB, pUC18::Δ*sbtAB*	SbtA-F SbtA-R	TAGGATCCAGACCTTAGCTATTACCAG ATGAATTCGATAAAACAGCATGGCAAC	1200 bp genomic fragment 3' of *sbtA*
	SbtB-F SbtB-R	TTGGATCCAGTCCCTTCCGCTAAAAG AAAAGCTTGGGGGTACTAGAGGTCAAC	1375 bp genomic fragment 3' of *sbtB*

[a] Primers used for amplification of genomic DNA from *Synechococcus elongatus* PCC7942.

[b] The *kan*^{R} and *cm*^{R} marker genes cassettes were inserted into the *cmpAB* genomic fragment and the *sbtA* and *sbtB* flanking regions, respectively, and cloned into the pUC18 vector.

Table 2. *E. coli* and cyanobacterial cell lines and plasmids used for protein expression and physiological analyses of the SbtA and SbtB proteins from *Cyanobium sp.* PCC7001 and *Synechococcus elongatus* PCC7942.

Organism	Plasmid::Gene(s) of interest [a]	Promoter(s)	Proteins expressed
E. coli DH5α	pSE2-1::*sbtAsbtBHAH6*-7942	*lacZ*	$SbtA_{7942}$ $SbtB_{7942}$-HAHis
E. coli DH5α	pSE2-1::*sbtAsbtBHAH5*-7001	*lacZ*	$SbtA_{7001}$ $SbtB_{7001}$-HAHis
Synechococcus ΔCS	pSE4-1::*sbtA*-7942	*native sbtAB-7942* [b]	$SbtA_{7942}$
Synechococcus ΔCS	pSE4-1::*sbtAsbtbB*-7942	*native sbtAB-7942* [b]	$SbtA_{7942}$ $SbtB_{7942}$
Synechococcus ΔCS	pSE4-1::*sbtAsbtBHAH6*-7942	*native sbtAB-7942* [b]	$SbtA_{7942}$ $SbtB_{7942}$-HAHis
Synechococcus ΔCS	pSE4-1::*sbtAsbtBHAH6*-7001	*native sbtAB-7001* [c]	$SbtA_{7001}$ $SbtB_{7001}$-HAHis

[a] pSE2-1 and pSE4-1 contain a spectinomycin resistance cassette (sp^R) for selection.

[b] *sbtA*-7942 and *sbtB*-7942 are transcribed in opposite directions away from each other. The intergenic region between the ATG-translation start codons contains used for expression contains the promoters both genes.

[c] *sbtA*-7001 and *sbtB*-7001 are transcribed in the same direction in tandem. The promoter is contained within the 500 bp upstream of the GTG-translation start for *sbtA*.